

The Bethe Roots of Regge Cuts in Strongly Coupled $\mathcal{N} = 4$ SYM Theory

J. Bartels,^a V. Schomerus^b and M. Sprenger^{b,c}

^a*II. Institute for Theoretical Physics, Hamburg University,
Luruper Chaussee 149, 22671 Hamburg, Germany*

^b*DESY Hamburg, Theory Group,
Notkestraße 85, 22607 Hamburg, Germany*

^c*Institute for Theoretical Physics, ETH Zürich,
Wolfgang-Pauli-Strasse 27, 8093 Zürich, Switzerland*

E-mail: joachim.bartels@desy.de, volker.schomerus@desy.de,
sprengerm@itp.phys.ethz.ch

ABSTRACT: We describe a general algorithm for the computation of the remainder function for n -gluon scattering in multi-Regge kinematics for strongly coupled planar $\mathcal{N} = 4$ super Yang-Mills theory. This regime is accessible through the infrared physics of an auxiliary quantum integrable system describing strings in $\text{AdS}_5 \times \text{S}^5$. Explicit formulas are presented for $n = 6$ and $n = 7$ external gluons. Our results are consistent with expectations from perturbative gauge theory. This paper comprises the technical details for the results announced in [1].

KEYWORDS: AdS/CFT correspondence, scattering amplitudes, Bethe Ansatz

Contents

1	Introduction	2
2	Multi-Regge kinematics	3
2.1	Kinematic variables	3
2.2	The multi-Regge regime	5
2.3	Multi-Regge regions	7
2.4	Weak coupling results	9
3	Scattering amplitude at strong coupling	12
3.1	Amplitude and thermodynamic Bethe Ansatz	12
3.2	Approaching multi-Regge kinematics	15
3.3	Amplitude and multi-Regge Bethe Ansatz	16
4	Results for the 7-point amplitude	20
4.1	An alternative Y-system	21
4.2	Remainder function in the Regge region $(- - +)$	22
4.2.1	Numerical analysis of the continuation	22
4.2.2	Calculation of the remainder function	24
4.3	Remainder function in the Regge region $(- - -)$	27
4.3.1	Numerical analysis of the continuation	27
4.3.2	Calculation of the remainder function	29
4.4	Remainder function in the Regge region $(- + -)$	30
5	Conclusions and outlook	31
A	Conformal Gram relations	32
B	The remainder function in the Euclidean regime	35
C	Kernels of the rewritten Y-system	35
D	S-matrices	36
E	Remainder function in the Regge region $(+ - -)$	37

1 Introduction

One of the major goals of modern theoretical physics is to construct the exact S-matrix of a four-dimensional interacting quantum field theory. It is believed that $\mathcal{N} = 4$ super Yang-Mills (SYM) theory provides the simplest example for which this task may be achieved, at least in the planar limit. The first conjectured expression for gluon scattering amplitudes in this theory, known as the Bern-Dixon-Smirnov (BDS) formula [2], was shown to be incomplete for $n \geq 6$ external gluons beyond one-loop order [3–5]. The corrections to the BDS formula are captured by the so-called remainder function. For the maximally helicity violating (MHV) configuration the remainder function is known up to four loops [6–8] for six gluons and up to two loops [9, 10] for seven gluons.

While the construction of the leading loop corrections to the BDS formula is a remarkable achievement which is based on beautiful and non-trivial mathematical concepts, these expressions are still a long way from an all-loop result (although first all-loop proposals have started to emerge recently [11–14]). On the other hand, all-loop expressions do exist for the anomalous dimensions of local operators in $\mathcal{N} = 4$ super Yang-Mills theory [15–17]. In that case, the initial progress from perturbative field theory computations [18–20] was soon complemented by string theoretic calculations [21] which capture the behavior at strong coupling via the AdS/CFT correspondence [22–24]. It were these investigations at strong coupling, such as [25–29], that brought the breakthrough and paved the way for the first all-loop expressions of anomalous dimensions [30].

Given the way things developed for the anomalous dimensions it seems worthwhile to invest more effort into the study of scattering amplitudes in strongly coupled $\mathcal{N} = 4$ super Yang-Mills theory. All computations in this regime are based on the work of Alday and Maldacena [31] who propose that scattering amplitudes in strongly coupled $\mathcal{N} = 4$ super Yang-Mills theory are given by the area of a minimal surface in AdS_5 whose boundary is fixed to a piecewise light-like Wilson loop on the boundary of AdS_5 . In a series of papers [32–34] it is shown that this minimal area problem can be reformulated through a set of coupled non-linear integral equations, the so-called Y-system. These take a form which is familiar from the theory of one-dimensional quantum integrable models. They describe a system of excitations with certain masses and chemical potentials which live on a circle and which interact through an integrable $2 \mapsto 2$ scattering. The interaction is engineered in such a way that the free energy of this system exactly reproduces the area of the minimal surface and thereby elegantly computes the amplitude.

In general, scattering amplitudes of four-dimensional quantum field theories are complicated functions of the kinematical invariants and the coupling constants. While the ultimate goal is to determine the full dependence on all of these variables, it might pay off to consider special kinematical limits at first. There are several choices which are being considered. These include, for example, two-dimensional kinematics [35–38], the limit in which the boundary polygon becomes regular [34, 39–42] or the OPE limit of [11–13, 43–48]. In this work we shall study a well-known kinematical limit that has a long history in gauge theory, the multi-Regge limit.

The multi-Regge limit has received much attention for two important reasons. On the one hand, it describes real scattering events at high energies which are observed at particle colliders.

On the other hand, investigations in QCD revealed a second remarkable feature: It turns out that in the multi-Regge limit the quantities governing the scattering amplitude are controlled by the spectrum of an integrable spin chain [49, 50]. For $\mathcal{N} = 4$ super Yang-Mills theory, these quantities are by now known to third order in perturbation theory [4, 5, 8, 51–53] and for the six-gluon case an all-loop conjecture was recently put forward in [54]. Therefore, the situation somewhat mirrors the early development in the case of anomalous dimensions where the first few orders in perturbation theory were also controlled with the help of integrability.

Given this state of affairs it seems very natural to ask what the multi-Regge limit corresponds to on the strong coupling side. In [55, 56] we show that the multi-Regge limit of gauge theory corresponds to the infrared, or low temperature, limit of the Y-system. In such a low temperature limit, one can neglect the integral terms in the non-linear integral equations. What remains is a system of algebraic Bethe Ansatz equations which can be solved quite easily. The aim of this work is to explain these Bethe Ansatz equations and to explain how to construct the remainder functions from solutions of these equations. In order to illustrate the general algorithm we will then calculate the remainder function in multi-Regge kinematics for six and seven gluons. Our results are in agreement with features that are expected from the perturbative evaluation in the leading logarithmic approximation.

2 Multi-Regge kinematics

The aim of this section is to introduce the relevant kinematic invariants and to discuss their behavior in the multi-Regge limit. As is well known, the n -gluon remainder function depends on $3n - 15$ cross ratios. For our discussion of $2 \rightarrow n - 2$ production amplitudes, we shall need a particular set of such cross ratios. This is discussed in the first subsection. We then turn to the multi-Regge limit and describe how our basis of cross ratios behaves as we go to high energies. The multi-Regge limit is described by the neighborhood of a particular point in the space of cross ratios. In order to exhibit interesting multi-Regge behavior, we must take the limit in various regions. These are discussed in the third subsection.

2.1 Kinematic variables

A scattering process of n massless gluons is parametrized by kinematic invariants which can be built from products $p_i \cdot p_j$. After taking the on-shell conditions $p_i^2 = 0$ and momentum conservation into account, we count $D_n = \frac{1}{2}(n - 1)(n - 2) - 1$ such product invariants. But these are not all independent. In fact, they are still subject to Gram determinant relations. There are $g_n = \frac{1}{2}(n - 4)(n - 5)$ such relations which arise from the fact that at most four vectors can be linearly independent in four dimensions and are obtained from the various vanishing 5×5 subdeterminants of the $(n - 1) \times (n - 1)$ matrix $P_{ij} = (p_i \cdot p_j)$, for details see appendix A. This leaves us with $D_n - g_n = 3n - 10$ independent Mandelstam invariants which parametrize our scattering problem.

In order to describe the multi-Regge limit of a $2 \rightarrow n - 2$ production amplitude, we introduce the standard Mandelstam invariants,

$$\begin{aligned} s_{i,j} &= (p_i + \cdots + p_j)^2, & i = 3, \dots, n - 1, j = i + 1, \dots, n, \\ t_i &= (p_2 + \cdots + p_{i+2})^2, & i = 1, \dots, n - 3, \end{aligned} \tag{2.1}$$

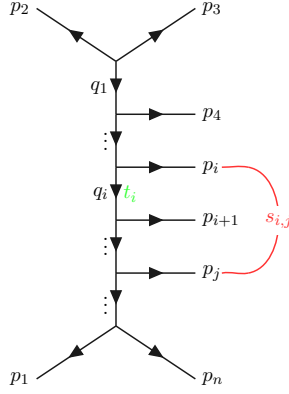


Figure 1. Graphical representation of the choice of Mandelstam variables as defined in Eq. (2.1).

where we choose all momenta to be outgoing, as shown in figure 1. Note that there are $n - 3$ t -like variables t_i and $\frac{1}{2}(n - 3)(n - 2)$ s -like invariants. The latter include all subenergies, starting from the variables $s_i = s_{i+2,i+3}$ with $i = 1, \dots, n - 3$ for pairs of outgoing particles up to the total energy $s = s_{3,n}$ of the process. The overall number of these variables is $(n - 3) + \frac{1}{2}(n - 3)(n - 2) = D_n$. One possible choice of independent kinematic invariants would include the $2n - 6$ variables t_i and s_i along with $n - 4$ variables η_a which are defined by

$$\eta_a := \frac{s_a s_{a+1}}{s_{a+2,a+4}}, \quad a = 1, \dots, n - 4. \quad (2.2)$$

These are directly related to the subenergies $s_{a+2,a+4}$ for three outgoing particles. All higher subenergies are then obtained from the t_i, s_i and η_a through the Gram determinant relations we described above.

Because of the dual conformal symmetry of $\mathcal{N} = 4$ super Yang-Mills theory, the remainder function depends on fewer parameters. To introduce the relevant variables, let us parametrize the momenta p_i through the dual variables $p_i =: x_{i-1} - x_i$, with $x_{i+n} = x_i$. The x_i are position variables for the cusps of a light-like Wilson loop describing our momentum configuration. Along with the x_i we also introduce $x_{i,j}^2 = (x_i - x_j)^2$ for $i, j = 1, \dots, n$, which are just the Mandelstam invariants introduced before. Note that $x_{i,i}^2 = x_{i,i+1}^2 = 0$, since we are considering a light-like Wilson loop. Hence, the $x_{i,j}^2$ provide $D_n = \frac{1}{2}n(n - 3)$ Mandelstam invariants which we may arrange in an $n \times n$ matrix $X_{ij} := (x_{i,j}^2)$. The $x_{i,j}^2$ possess a rather simple relation with the Mandelstam invariants we described above. In the case of $n = 7$ external gluons, for example, one has

$$X = \begin{bmatrix} 0 & 0 & x_{1,3}^2 & x_{1,4}^2 & x_{1,5}^2 & x_{1,6}^2 & 0 \\ 0 & 0 & 0 & x_{2,4}^2 & x_{2,5}^2 & x_{2,6}^2 & x_{2,7}^2 \\ x_{1,3}^2 & 0 & 0 & 0 & x_{3,5}^2 & x_{3,6}^2 & x_{3,7}^2 \\ x_{1,4}^2 & x_{2,4}^2 & 0 & 0 & 0 & x_{4,6}^2 & x_{4,7}^2 \\ x_{1,5}^2 & x_{2,5}^2 & x_{3,5}^2 & 0 & 0 & 0 & x_{5,7}^2 \\ & & & 0 & 0 & 0 & \\ & & & & 0 & 0 & \end{bmatrix} = \begin{bmatrix} 0 & 0 & t_1 & t_2 & t_3 & t_4 & 0 \\ 0 & 0 & 0 & s_1 & s_{3,5} & s_{3,6} & s \\ t_1 & 0 & 0 & 0 & s_2 & s_{4,6} & s_{4,7} \\ t_2 & s_1 & 0 & 0 & 0 & s_3 & s_{5,7} \\ t_3 & s_{3,4} & s_2 & 0 & 0 & 0 & s_4 \\ & & & & 0 & 0 & 0 \\ & & & & & 0 & 0 \end{bmatrix}, \quad (2.3)$$

where the entries not shown can be obtained by the symmetry $X_{ij} = X_{ji}$. For other numbers n of external gluons, the relations take a similar form, with t -like variables in the first row and all the s -like variables filling a triangle in row 2 to $n - 2$.

From these Mandelstam invariants we can easily construct $D_n - n$ dual conformal invariant quantities

$$U_{ij} = \frac{x_{i,j+1}^2 x_{i+1,j}^2}{x_{i,j}^2 x_{i+1,j+1}^2}, \quad (2.4)$$

which are called cross ratios. Once again, these are not all independent. Additional relations are obtained from the $c_n = \frac{1}{2}(n - 5)(n - 6)$ conformal Gram relations which state that all 7×7 subdeterminants of the matrix X must vanish (cf. appendix A). They leave us with $D_n - n - c_n = 3n - 15$ independent cross ratios.

As in our discussion of independent Mandelstam invariants, it is useful to fix an independent set of cross ratios which is adapted to the multi-Regge limit of a $2 \rightarrow n - 2$ production amplitude. In [56] we suggest to use

$$u_{1\sigma} = U_{\sigma+1,\sigma+4} = \frac{x_{\sigma+1,\sigma+5}^2 x_{\sigma+2,\sigma+4}^2}{x_{\sigma+2,\sigma+5}^2 x_{\sigma+1,\sigma+4}^2}, \quad (2.5)$$

$$u_{2\sigma} = U_{\sigma+2,n} = \frac{x_{\sigma+3,n}^2 x_{1,\sigma+2}^2}{x_{\sigma+2,n}^2 x_{1,\sigma+3}^2}, \quad (2.6)$$

$$u_{3\sigma} = U_{1,\sigma+3} = \frac{x_{2,\sigma+3}^2 x_{1,\sigma+4}^2}{x_{2,\sigma+4}^2 x_{1,\sigma+3}^2}, \quad (2.7)$$

where $\sigma = 1, \dots, n - 5$. All other cross ratios, and in particular those defined in Eq. (2.4), may be reconstructed from the $u_{a\sigma}$ by solving the conformal Gram determinant relations (see appendix A for the unique Gram relation in the 7-gluon case). A convenient graphical representation of the cross ratios Eqs. (2.5)-(2.7) is shown in figure 2. A symmetry we will use later is target-projectile symmetry, which, as the name suggests, reflects the fact that the amplitude should remain invariant when the two incoming particles p_1, p_2 are swapped. In terms of the graphical representation of the cross ratios in figure 2, target-projectile symmetry simply amounts to a reflection on the central vertical axis of each blob. From this, it is easy to deduce that applying target-projectile symmetry amounts to the following exchange of cross ratios

$$u_{1\sigma} \leftrightarrow u_{1(n-4-\sigma)}, \quad u_{2\sigma} \leftrightarrow u_{3(n-4-\sigma)}. \quad (2.8)$$

2.2 The multi-Regge regime

By definition, the multi-Regge regime is reached when we impose a strong ordering of the rapidities of the outgoing particles p_3, \dots, p_n while keeping their transverse momenta of the same order. For the Mandelstam variables this translates into all s -like variables becoming large with t -like variables fixed. More precisely, we get a hierarchy

$$s = s_{3,n} \gg s_{3,n-1}, s_{4,n} \gg \dots \gg s_{i,i+2} \gg s_i \gg -t_i. \quad (2.9)$$

In terms of the matrix X_{ij} introduced in Eq. (2.3) this means that the s -like variables become larger as we go to the upper right corner. This scaling of kinematic invariants is discussed in

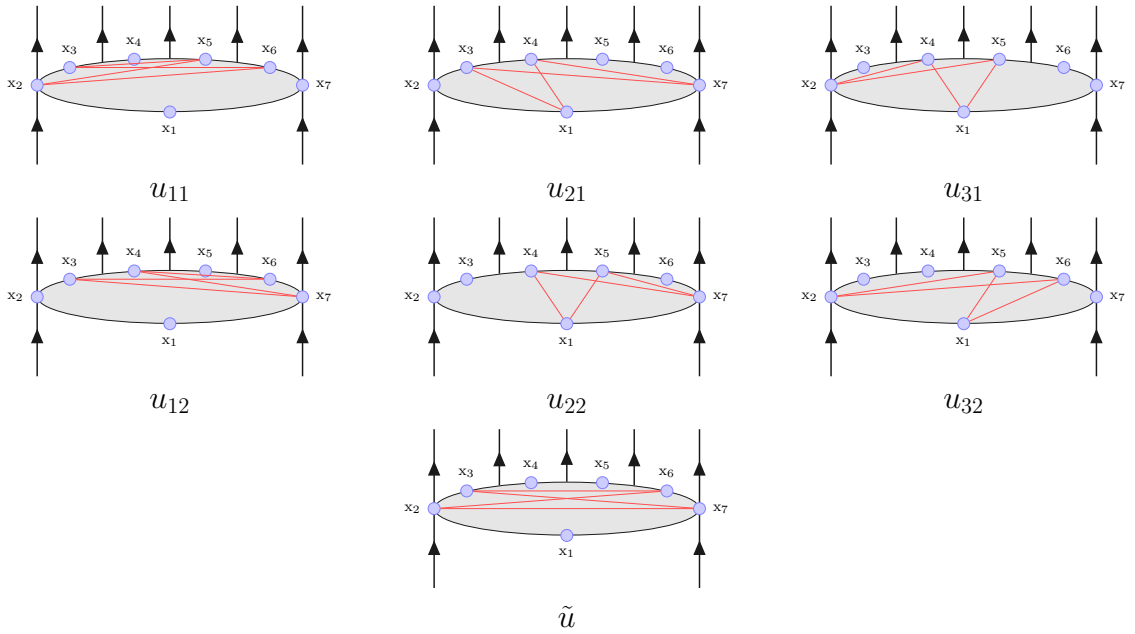


Figure 2. Graphical representation of the cross ratios for the 7-gluon amplitude. The cross ratios u_{as} are chosen to be independent (cf. Eqs. (2.5)-(2.7)), while \tilde{u} depends on those cross ratios through a conformal Gram relation.

more detail in [56]. In the limiting regime one finds that

$$x_{ij}^2 = s_{i+1,j} \sim s_{i-1} \cdots s_{j-3} . \quad (2.10)$$

As we can easily infer from Eq. (2.10) and our definition of the independent cross ratios (2.5)-(2.7), the limiting behavior of the $u_{a\sigma}$ is therefore given by

$$u_{2\sigma} \sim \frac{1}{s_{\sigma+1}}, \quad u_{3\sigma} \sim \frac{1}{s_{\sigma+1}}, \quad 1 - u_{1\sigma} \sim \frac{1}{s_{\sigma+1}} . \quad (2.11)$$

Hence, the approach to the multi-Regge limit is characterized by the finite, reduced cross ratios

$$\tilde{u}_{2\sigma} := \frac{u_{2\sigma}}{1 - u_{1\sigma}} =: \frac{1}{|1 + w_\sigma|^2}, \quad \tilde{u}_{3\sigma} := \frac{u_{3\sigma}}{1 - u_{1\sigma}} =: \frac{|w_\sigma|^2}{|1 + w_\sigma|^2}, \quad (2.12)$$

where we introduced the complex quantities w_σ as in [52]. Let us note that the other cross ratios U_{ij} with $i > 1$ and $j < n$ possess the limiting behavior

$$U_{ij} - 1 \sim s_i^{-1} \cdots s_{j-3}^{-1} . \quad (2.13)$$

For example, in the case of $n = 7$ we can easily see that $\tilde{u} := U_{26}$ approaches 1 in the multi-Regge limit, as it must in order to satisfy the conformal Gram relation we spell out in appendix A. In fact, inserting $u_{1\sigma} = 1$ and $u_{2\sigma} = u_{3\sigma} = 0$ into Eq. (A.9) leads to the Gram relation $(\tilde{u} - 1)^2 = 0$.

2.3 Multi-Regge regions

As we shall discuss below, it is very important to evaluate the multi-Regge limit in different kinematical regions. In fact, in the so-called Euclidean region where all kinematic invariants are negative, the multi-Regge limit of the remainder function vanishes. If this was the only admissible regime, the multi-Regge limit would be incapable of distinguishing between the BDS Ansatz and the true scattering amplitude. Fortunately, we have more freedom in taking the multi-Regge limit.

In the Euclidean region, the energy components p_i^0 of the four-momenta p_i of the produced particles are taken to be positive. In other words, all the p_i take values in the forward light cone. But we can admit different choices for the sign of p_i^0 . These characterize 2^{n-4} admissible kinematical regions¹. Let us define an associated map

$$\varrho_i = \text{sgn}(p_i^0) \in \{\pm 1\}, \quad (2.14)$$

by which we parametrize the region $(\varrho_4 \cdots \varrho_{n-1})$. It is possible to characterize the regions through the behavior of Mandelstam invariants and cross ratios. For the Mandelstam invariants, the t -like variables remain negative while s -like variables may change sign. Because of Eq. (2.10), the approach to the multi-Regge limit is characterized by the following behavior

$$\varrho_i \varrho_j s_{i,j} \geq 0 \quad (2.15)$$

with $\varrho_3 = \varrho_n = 1$. Furthermore, note that the sign of the s -like variables is uniquely characterized by the signs of the two-particle invariants s_i , using the multi-Regge behavior (2.10).

Let us now pass to the cross ratios. In the Euclidean regime, all cross ratios are positive since they involve an even number of t -like invariants. But once we pass to other regions, the cross ratios $u_{2\sigma}$ and $u_{3\sigma}$ may change signs according to the rules

$$\varrho_{\sigma+3} \varrho_{\sigma+4} u_{2\sigma} \geq 0, \quad \varrho_{\sigma+3} \varrho_{\sigma+4} u_{3\sigma} \geq 0, \quad (2.16)$$

where $\sigma = 1, \dots, n-5$. Note that the signs of these cross ratios are not sufficient to specify the regime as they leave one sign undetermined.

We can pass from one multi-Regge region to another by analytic continuation in the kinematic invariants. In going from the Euclidean region with all the $u_{a\sigma}$ positive to another region that is characterized by factors ϱ_i , we shall use a curve for which the cross ratios U_{ij} possess non-vanishing winding number n_{ij} around $U_{ij} = 0$. This winding number is related to the parameters ϱ_i through²

$$n_{ij} = \frac{1}{4}(\varrho_{i+1} - \varrho_{i+2})(\varrho_j - \varrho_{j+1}). \quad (2.17)$$

Winding number $n = 1$ means that we encircle the origin of the U-plane in clockwise direction, while $n = -1$ corresponds to a counter-clockwise rotation. The formula for n_{ij} can be used for all $i, j = 1, \dots, n$ if we extend the definition of ϱ_i such that $\varrho_1 = \varrho_2 = \varrho_{n+1} = \varrho_{n+2} = 2$. For the

¹In this paper, we consider only those regions for which the energy component of the momenta p_3 and p_n remains positive. It should be noted that changing the sign of the energy component of those particles is possible as well and considered for example in [57].

²This formula is simple to derive when using that the winding number of $s_{i,j}$ is given by $\frac{1}{2}(1 - \varrho_i \varrho_j)$.

small cross ratios $u_{2\sigma} = U_{\sigma+2,n}$ and $u_{3\sigma} = U_{1,\sigma+3}$ the winding number n_{ij} is given by $\pm\frac{1}{2}$. The winding numbers for all other cross ratios are integer valued, i.e. these cross ratios perform full rather than half rotations.

The precise curve along which we perform the continuation must be constructed such that

- all winding numbers assume the prescribed values (2.17) and
- all conformal Gram determinant relations are respected.

For the cross ratios $u_{2\sigma}$ and $u_{3\sigma}$ we propose the following simple behavior

$$u_{2\sigma}(\varphi) = e^{\frac{i}{2}(\varrho_{\sigma+3}-\varrho_{\sigma+4})\varphi} u_{2\sigma}, \quad u_{3\sigma}(\varphi) = e^{\frac{i}{2}(\varrho_{\sigma+4}-\varrho_{\sigma+3})\varphi} u_{3\sigma}, \quad (2.18)$$

where $\varphi \in [0, \pi]$ parametrizes the curve along which we continue. This is the simplest behavior that is consistent with our formula (2.17) and it changes the signs of the cross ratios $u_{2\sigma}$ and $u_{3\sigma}$ such that we end up in the desired region, see Eq. (2.16). For all other cross ratios the dependence on φ is more complicated, at least in general. The simplest curves that possess the correct winding numbers are, of course, circles. However, as we shall see in some examples below, having all the cross ratios move along circles is rarely ever consistent with the Gram relations.

Let us consider some specific examples. In the case of $n = 6$ we have four multi-Regge regions including the Euclidean one. Hence there are three non-trivial paths connecting the Euclidean region to the three others. These are given by

$$P_{6,+ -} : u_{11}(\varphi) = u_{11}, \quad u_{21}(\varphi) = e^{i\varphi} u_{21}, \quad u_{31}(\varphi) = e^{-i\varphi} u_{31} \quad (2.19)$$

$$P_{6,- +} : u_{11}(\varphi) = u_{11}, \quad u_{21}(\varphi) = e^{-i\varphi} u_{21}, \quad u_{31}(\varphi) = e^{i\varphi} u_{31} \quad (2.20)$$

$$P_{6,- -} : u_{11}(\varphi) = e^{-2i\varphi} u_{11}, \quad u_{21}(\varphi) = u_{21}, \quad u_{31}(\varphi) = u_{31}, \quad (2.21)$$

where the subscript \pm indicates the signs of the energies we choose for the produced particles. Since there are no further cross ratios and no conformal Gram relations to satisfy, it is obvious that our three curves possess all the desired properties.

If we choose $n = 7$ there are eight multi-Regge regions. One is the Euclidean region, three others correspond to a single change of signs. For the latter, none of the integer winding numbers n_{ij} with $i > 1$ and $j < n$ is actually non-zero. Such curves will turn out to lead to regions with trivial Regge limit, both at weak and strong coupling. It therefore suffices to discuss the remaining four curves. Extending our general prescription in Eq. (2.18), the first three of them are given by

$$P_{7,+ - -} : u_{11}(\varphi) = u_{11}, \quad u_{21}(\varphi) = e^{i\varphi} u_{21}, \quad u_{31}(\varphi) = e^{-i\varphi} u_{31}, \quad (2.22)$$

$$u_{12}(\varphi) = e^{-2i\varphi} u_{12}, \quad u_{22}(\varphi) = u_{22}, \quad u_{32}(\varphi) = u_{32}, \quad \tilde{u}(\varphi) = \tilde{u}$$

$$P_{7,- + -} : u_{11}(\varphi) = e^{2i\varphi} u_{11}, \quad u_{21}(\varphi) = e^{-i\varphi} u_{21}, \quad u_{31}(\varphi) = e^{i\varphi} u_{31}, \quad (2.23)$$

$$u_{12}(\varphi) = e^{2i\varphi} u_{12}, \quad u_{22}(\varphi) = e^{i\varphi} u_{22}, \quad u_{32}(\varphi) = e^{-i\varphi} u_{32}, \quad \tilde{u}(\varphi) = e^{-2i\varphi} \tilde{u}$$

$$P_{7,- - +} : u_{11}(\varphi) = e^{-2i\varphi} u_{11}, \quad u_{21}(\varphi) = u_{21}, \quad u_{31}(\varphi) = u_{31}, \quad (2.24)$$

$$u_{12}(\varphi) = u_{12}, \quad u_{22}(\varphi) = e^{-i\varphi} u_{22}, \quad u_{32}(\varphi) = e^{i\varphi} u_{32}, \quad \tilde{u}(\varphi) = \tilde{u} .$$

It should be noted that the paths spelled out above satisfy the Gram relation only in the multi-Regge limit, i.e. when Eq.(2.11) holds. This, however, is satisfied for all cases studied in this paper. In order to reach the forth region, in which all $\varrho_i = -1$, the conformal Gram relations force us to consider a more complicated curve. It is still easy to give an explicit expression in the limit where $u_{2\sigma} = u_{3\sigma} = 0$,

$$\begin{aligned}
P_{7,---} : u_{11}(\varphi) &= e^{2i\varphi} \left(1 - \sqrt{1 - e^{-2i\varphi}}\right) u_{11}, & u_{21}(\varphi) &= u_{21}, & u_{31}(\varphi) &= u_{31}, \\
u_{12}(\varphi) &= e^{2i\varphi} \left(1 - \sqrt{1 - e^{-2i\varphi}}\right) u_{12}, & u_{22}(\varphi) &= u_{22}, & u_{32}(\varphi) &= u_{32}, & \tilde{u}(\varphi) &= e^{-2i\varphi} \tilde{u}.
\end{aligned}
\tag{2.25}$$

In the multi-Regge limit, the parameters $u_{2\sigma}, u_{3\sigma}$ become small so that P_{---} is a good approximation. This last path illustrates nicely that one cannot always analytically continue along circles. Just computing the winding numbers for this path, we find that the cross ratios $u_{a\sigma}$ we choose as independent variables have winding number zero, while the cross ratio \tilde{u} , which is given in terms of the independent cross ratios via the conformal Gram relation, has winding number $\tilde{n} = +1$. This is impossible to realize with $u_{1\sigma}(\varphi) = u_{1\sigma}$ constant because the conformal Gram relations would force \tilde{u} to be constant, as well. Choosing the path for \tilde{u} to run along a circle, as we did in our prescription for $P_{7,---}$, we can solve Eq. (A.11) for u_{11}, u_{12} while preserving the target-projectile symmetry along the entire path. This leads to the expressions we have prescribed. Note that the Gram determinant relation (A.11) has been derived with the additional assumption that $u_{2\sigma} = u_{3\sigma} = 0$. Hence, our curve $P_{7,---}$ is only valid in the multi-Regge limit.

2.4 Weak coupling results

On the weak coupling side, soon after the BDS conjecture for the planar n -point scattering amplitude had been published, it became clear that for more than five external legs the BDS formula is incomplete. The missing pieces are encoded in the remainder functions, R_n , and in recent years intense work has been devoted to the calculation of these functions. The multi-Regge limit provides enormous help in determining R_n .

Starting point is the multi-Regge analysis of the $2 \rightarrow 4$ scattering amplitude in the leading logarithmic approximation. In [4, 5] it is shown that the failure of the BDS formula is due to the existence of Regge cut contributions. More precisely, the perturbative analysis shows that the high-energy behavior of the $2 \rightarrow 4$ scattering process is described by the exchange of Regge poles - the reggeized gluon - and a Regge cut consisting of the exchange of two interacting reggeized gluons. In the planar approximation this cut is present only in specific kinematic regions which have been named Mandelstam regions. The BDS formula does not account for this Regge cut contribution. As shown in [4], it contains the Regge poles, and the phase structure is correct in the Euclidean region (where all energies are negative) and in the physical region where all energies are positive. In the Mandelstam region where the Regge cut appears in the perturbative analysis, the BDS formula exhibits a phase which has been identified as the one-loop part of the Regge cut contribution. At the same time, in these kinematic regions the phase structure of the Regge pole contributions is not correctly reproduced by the BDS formula [58].

In fact, there is a close connection between the structure of Regge pole contribution and the existence of Regge cut contributions [57]. In the planar approximation, the Regge pole

expression for the $2 \rightarrow n - 2$ amplitude has a simple factorizing form in only some kinematic regions, such as the Euclidean region or the region of positive energies. In contrast, just in those kinematic regions where the Regge cut contributions are present, the Regge pole expressions develop unphysical singularities which have to be canceled by the Regge cut singularities. The existence of Regge cuts, therefore, is required to provide a consistent (i.e. singularity-free and, in the case of $\mathcal{N} = 4$ SYM, also conformally invariant) description of Regge poles.

The general analysis of the structure of the Regge pole contributions in $2 \rightarrow n - 2$ scattering amplitudes is presented in [57]. In particular, this analysis allows to find the analytic form of the Regge pole contributions for planar amplitudes in all kinematic regions, including the singular pieces which have to be canceled by the Regge cut contributions. Details are worked out for the cases $2 \rightarrow 4$ and $2 \rightarrow 5$ in [57], and in [59] for the case $2 \rightarrow 6$.

The calculation of the Regge cut contributions is based upon the calculation of energy discontinuities using unitarity integrals. In order to obtain energy discontinuities one needs the analytic representation of the scattering amplitudes in multi-Regge kinematics which, in agreement with the Steinmann relations, exhibits the dependence upon the energy variables, including the phases in the different kinematic regions. The authors of [60] outline a general strategy for the calculation of Regge cut contributions. These contain the singular terms which exactly cancel the singular terms of the Regge pole contributions: when pole and cuts are combined one finds a sum of infrared finite and conformally invariant pole and cut expressions. Explicit leading order result for the $2 \rightarrow 5$ and $2 \rightarrow 6$ cases are obtained in [60] and [59], respectively.

Let us briefly summarize some of those results which are of special interest for the analysis described in this paper. To be complete we begin with the $2 \rightarrow 4$ case. The Regge cut appears in the kinematic region $(--)$: this is the one which is studied in [55] and it is contained in the list (2.19) - (2.21). In terms of Mandelstam variables the energies have the following sign structure

$$s, s_2 > 0, s_1, s_3, s_{3,5}, s_{4,6} < 0 . \quad (2.26)$$

Note that there is a second region, not mentioned in the above list, in which the cut appears: it is obtained by ‘twisting’ the t_2 channel. The other two regions, $(+-)$ and $(-+)$, do not contain the Regge cut contribution. The corresponding path of analytic continuation for the region $(--)$ is described in Eq. (2.21). It is possible to define other, more complicated paths which connect the same starting and final values of energies, but the path Eq. (2.21) appears to be the simplest one. The Regge cut amplitude which emerges after combination with the Regge pole contribution is derived in [5] and the full remainder function in this region is obtained in [60]:

$$\left[e^{R_6 + i\delta_{6,--}} \right]_{--} = \cos \pi \omega_{ab} + i\delta_{6,--} + 2i f_{\omega_2} . \quad (2.27)$$

In terms of the cross ratios the cut amplitude f_{ω_2} has the form:

$$f_{\omega_2} = \frac{g^2 N_c}{16\pi^2} \sum_n (-1)^n \left(\frac{w}{w^*} \right)^{\frac{n}{2}} \int \frac{d\nu}{2\pi i} \Phi_{\nu,n}^* \left[(-\sqrt{u_2 u_3})^{-\omega(\nu,n)} - 1 \right] \Phi_{\nu,n} |w|^{2i\nu} , \quad (2.28)$$

where $w = w_1$ was introduced in Eq. (2.12). Here $\Phi_{\nu,n}$ denotes the impact factor and $\omega(\nu, n)$ is the eigenvalue function of the color octet BFKL Hamiltonian. These quantities are known up

to next-to-leading order from direct field theory calculations [5, 51, 52]. Using the bootstrap program of [7, 8], the BFKL eigenvalue and the impact factor can be determined up to NNLLA and N³LLA, respectively, and all-order expressions derived from the Wilson loop OPE are put forward in [48].

In [62] it is shown that the BFKL Hamiltonian is equivalent to the non-compact $SL(2, C)$ Heisenberg Hamiltonian for an open spin chain, with $\omega(\nu, n)$ being the eigenvalue function for the spin chain of length two.

Next we turn to the case $2 \rightarrow 5$ [60]. Here, the weak-coupling analysis leads to three different Regge cut contributions composed of two reggeized gluons, two ‘short’ cuts in the t_2 and t_3 channels, respectively, and one ‘long cut’ extending over the t_2 and the t_3 channels. The different kinematic regions in which these cuts appear are listed in Eqs. (2.22)-(2.25), together with simple choices of paths of analytic continuation. The simplest cases are $(+ - -)$ and $(- - +)$: they contain only the short cuts in the t_3 and the t_2 channels, respectively. In these regions the remainder function has the following form

$$\left[e^{R_7 + i\delta_{7,+--}} \right]_{+--} = \cos \pi \omega_{bc} + i\delta_{7,+--} + 2i f_{\omega_3} \quad (2.29)$$

$$\left[e^{R_7 + i\delta_{7,-++}} \right]_{--++} = \cos \pi \omega_{ab} + i\delta_{7,-++} + 2i f_{\omega_2} \quad (2.30)$$

The integral expressions for the Regge cut amplitudes f_{ω_2} and f_{ω_3} are easily obtained from Eq. (2.28) by substituting the cross ratios $u_i \rightarrow u_{i\sigma}$. For the remaining two regions also the long cut contributes. For $(- - -)$ and $(- + -)$ the remainder functions are given by

$$\left[e^{R_7 + i\delta_{7,---}} \right]_{---} = \cos \pi \omega_{ac} + i\delta_{7,---} + 2i f_{\omega_2 \omega_3} \quad (2.31)$$

$$\left[e^{R_7 + i\delta_{7,-+-}} \right]_{-+-} = e^{i\pi \omega_{ba}} e^{i\pi \omega_{bc}} + i\delta_{7,-+-} + 2i(f_{\omega_2 \omega_3} - e^{i\pi \omega_{bc}} f_{\omega_2} - e^{i\pi \omega_{ba}} f_{\omega_3}). \quad (2.32)$$

The integral for the long cut reads

$$f_{\omega_2 \omega_3} = \frac{a}{2} \sum_{n_1, n_2} (-1)^{n_1 + n_2} \left(\frac{w_1}{w_1^*} \right)^{n_1} \left(\frac{w_2}{w_2^*} \right)^{n_2} \int \frac{d\nu_1 d\nu_2}{(2\pi)^2} \Phi(\nu_1, n_1)^* |w_1|^{2i\nu_1} (-\sqrt{u_{21} u_{31}})^{-\omega(\nu_1, n_1)} \\ C(\nu_1, \nu_2, n_1, n_2) (-\sqrt{u_{22} u_{32}})^{-\omega(\nu_2, n_2)} |w_2|^{2i\nu_2} \Phi(\nu_2, n_2)|_{\text{sub}}. \quad (2.33)$$

Here the impact factor $\Phi(\nu, n)$ is the same as in Eq. (2.28), and $C(\nu_1, \nu_2, n_1, n_2)$ stands for the central production vertex. The latter is known in leading order [61]. The subscript $|_{\text{sub}}$ indicates that we have subtracted the one-loop contribution. In [60] a few more kinematic regions with Regge cut contributions are listed; they will not be mentioned here.

It is important to note that in leading order the integral representation is real-valued up to the phase factors $e^{-i\pi \omega(\nu_i, n_i)}$. Beyond leading order this will no longer be the case. As explained in [60], one can still write the Regge cut amplitude in the form of Eq. (2.33), but with a complex-valued expression for the production vertex C . Alternatively, the amplitude breaks into two pieces with different phase factors.

Before we turn to the strong coupling regime let us make a final remark on the weak coupling results summarized in this section. Comparing the results for the $2 \rightarrow 4$ scattering amplitude

with those of the $2 \rightarrow 5$ case we would like to stress the close connections. Obviously the short Regge cuts in the $2 \rightarrow 5$ case have the same functional form as the $2 \rightarrow 4$ cut contribution (with suitable replacements of the cross ratios), i.e. the same impact factor and eigenvalue function $\omega(\nu, n)$. Also the expression for the long cut contains - apart from the new production vertex - the same building blocks.

New elements appear in the $2 \rightarrow 6$ scattering amplitude: in the region $(- + + -)$ one finds a Regge cut consisting of three reggeized gluons. Apart from a new impact factor, a new eigenvalue function $\omega_3(\nu_1, n_1; \nu_2, n_2)$ appears which belongs to a spin chain of length three and can be parametrized by two sets of conformal quantum numbers. In leading order this eigenvalue function can be written as a sum of the two functions $\omega(\nu_1, n_1)$ and $\omega(\nu_2, n_2)$ [62, 63]. Whether this simple additivity remains valid also beyond leading order is presently not known.

3 Scattering amplitude at strong coupling

In this section we shall outline the general algorithm for the calculation of the remainder function of strongly coupled $\mathcal{N} = 4$ SYM in the multi-Regge limit. All the key elements of our description are applicable for any number n of external gluons. There are a few formulas that we shall only spell out for $n = 7$ because their precise form for other values of n is irrelevant both for the presentation of the general algorithm and for the example we shall work out in the next section. After reviewing the form of the scattering amplitude and its relation with a special set of thermodynamic Bethe Ansatz equations, we will discuss how to perform the multi-Regge limit. In particular we shall show that the multi-Regge limit is a particular large mass limit in the underlying thermodynamic Bethe Ansatz. In such a large mass limit, the thermodynamic Bethe Ansatz equations get replaced by a much simpler set of algebraic Bethe Ansatz equations. The latter will be described explicitly in the third subsection. We conclude the section by illustrating the general algorithm through the simplest example, namely the case of $n = 6$ gluons, and explain how to evaluate the various contributions to the remainder function in the multi-Regge limit. For the least trivial contribution to the remainder function this will lead to a set of Bethe Ansatz equations. Special solutions of these Bethe Ansatz equations are associated with the various kinematical regions discussed above.

3.1 Amplitude and thermodynamic Bethe Ansatz

The problem of calculating strong coupling scattering amplitudes to leading order was solved in a series of papers [31–34], the solution of which we will briefly review here.

It turns out that the leading order of the n -gluon scattering amplitude can be written as

$$\mathcal{A} \sim e^{-\frac{\sqrt{\lambda}}{2\pi}A} = e^{-\frac{\sqrt{\lambda}}{2\pi}A_{\text{BDS}+R}} \quad (3.1)$$

where the quantity A consists of several different terms³ to be discussed one by one,

$$A = A_{\text{div}} + A_{\text{free}} + A_{\text{BDS-like}} + A_{\text{per}} . \quad (3.2)$$

³For the special case $n = 4k$ there is an additional contribution A_{extra} which is worked out in detail in [64]. Since this case is not considered in this paper, we drop this contribution in Eq.(3.1).

Let us discuss the four different contributions in the order of their appearance. To begin with, A_{div} encodes the infrared divergences of the amplitude and it reads

$$A_{\text{div}} = \frac{1}{8} \sum_i \log^2(\varepsilon^2 x_{i,i+2}^2), \quad (3.3)$$

where ε is a radial cutoff for AdS_5 . The next term A_{free} is the most interesting and least trivial one. As we anticipated in the introduction, it is constructed from a one-dimensional auxiliary quantum integrable system. For the n -gluon amplitude, it is defined in terms of $3n - 15$ functions, $Y_{a,s}(\theta)$, where $a = 1, 2, 3$ and $s = 1, \dots, n - 5$. These functions are determined by a set of non-linear integral equations, called the Y-system equations,

$$\log Y_{1,s} = -m_s \cosh \theta - C_s - \frac{1}{2} K_2 \star \beta_s - K_1 \star \alpha_s - \frac{1}{2} K_3 \star \gamma_s, \quad (3.4)$$

$$\log Y_{2,s} = -m_s \sqrt{2} \cosh \theta - K_2 \star \alpha_s - K_1 \star \beta_s, \quad (3.5)$$

$$\log Y_{3,s} = -m_s \cosh \theta + C_s - \frac{1}{2} K_2 \star \beta_s - K_1 \star \alpha_s + \frac{1}{2} K_3 \star \gamma_s, \quad (3.6)$$

where m_s and C_s are parameters that one can think of as mass parameters and chemical potentials of excitations in the one-dimensional auxiliary quantum system. The objects $\alpha_s, \beta_s, \gamma_s$ that appear on the right hand side are defined in terms of the functions $Y_{a,s}$ as

$$\alpha_s = \log \frac{(1 + Y_{1,s})(1 + Y_{3,s})}{(1 + Y_{2,s-1})(1 + Y_{2,s+1})}, \quad (3.7)$$

$$\beta_s = \log \frac{(1 + Y_{2,s})^2}{(1 + Y_{1,s-1})(1 + Y_{1,s+1})(1 + Y_{3,s-1})(1 + Y_{3,s+1})}, \quad (3.8)$$

$$\gamma_s = \log \frac{(1 + Y_{1,s-1})(1 + Y_{3,s+1})}{(1 + Y_{1,s+1})(1 + Y_{3,s-1})}. \quad (3.9)$$

In the Y-system these combinations of Y-functions are convoluted with the following simple kernel functions

$$K_1 = \frac{1}{2\pi} \frac{1}{\cosh \theta}, \quad K_2 = \frac{\sqrt{2}}{\pi} \frac{\cosh \theta}{\cosh 2\theta}, \quad K_3 = \frac{i}{\pi} \tanh 2\theta. \quad (3.10)$$

These kernel functions can be thought of as describing the (integrable) interaction between the excitations of the auxiliary quantum system. Let us also recall that the convolution product is defined as

$$(K * f)(\theta) = \int_{-\infty}^{\infty} d\theta' K(\theta - \theta') f(\theta'). \quad (3.11)$$

The spectral parameter θ in the Y-system equations is a complex variable. From the definition (3.10) of the kernel functions it is clear that for certain values of θ , the kernels can become singular. Therefore, the form of the Y-system as presented in Eqs. (3.4)-(3.6) is only valid for

$|\text{Im } \theta| \leq \frac{\pi}{4}$. If we wish to evaluate the Y-system for larger imaginary parts of θ , we have to pick up residues or use a powerful recursion relation for the Y-functions,

$$Y_{a,s}^{[r]} = \frac{\left(1 + Y_{a,s+1}^{[r+1]}\right) \left(1 + Y_{4-a,s-1}^{[r+1]}\right)}{Y_{4-a,s}^{[r+2]} \left(1 + \frac{1}{Y_{a+1,s}^{[r+1]}}\right) \left(1 + \frac{1}{Y_{a-1,s}^{[r+1]}}\right)}, \quad (3.12)$$

where $Y_{a,s}^{[r]}(\theta) = Y_{a,s}(\theta + ir\pi/4)$ denotes a shift in θ by a multiple of $i\frac{\pi}{4}$. When using the recursion relation, it should be noted that $Y_{0,s} = Y_{4,s} = \infty$, as well as $Y_{a,0} = Y_{a,n-4} = 0$.

An additional modification of the Y-system equations has to be made when the parameters m_s become complex, i.e. $m_s = |m_s|e^{i\phi_s}$. In this case, we have to substitute

$$m_s \rightarrow |m_s|, \quad Y_{a,s}(\theta) \rightarrow \tilde{Y}_{a,s}(\theta) := Y_{a,s}(\theta + i\phi_s), \quad (3.13)$$

$$K_{s,s'}^{a,a'}(\theta - \theta') \rightarrow K_{s,s'}^{a,a'}(\theta - \theta' + i(\phi_s - \phi_{s'})), \quad (3.14)$$

in Eqs. (3.4)-(3.6), as is shown in [34]. Once we solve the Y-system equations for the $\tilde{Y}_{a,s}$, we can finally calculate A_{free} , which reads

$$A_{\text{free}} = \sum_s \int \frac{d\theta}{2\pi} |m_s| \cosh \theta \left[\left(1 + \tilde{Y}_{1,s}\right) \left(1 + \tilde{Y}_{3,s}\right) \left(1 + \tilde{Y}_{2,s}\right)^{\sqrt{2}} \right] (\theta). \quad (3.15)$$

The expression resembles similar formulas for the free energy in one-dimensional integrable quantum systems. As it stands, the expression for A_{free} provides a function of the system parameters m_s , C_s and ϕ_s . We shall review below how these are related to the physical cross ratios.

There are two additional terms in the general expression (3.2) for the logarithm of the scattering amplitude, namely $A_{\text{BDS-like}}$ and A_{per} . These are again much simpler to spell out than A_{free} and although they are known for any number n of gluons, we shall content ourselves with the expressions for $n = 7$. In this case, $A_{\text{BDS-like}}$ can be written as

$$A_{\text{BDS-like}} = -\frac{1}{4} \sum_{i=1}^7 \left(\log^2 x_{i,i+2}^2 + \sum_{k=0}^2 (-1)^{k+1} \log x_{i,i+2}^2 \log x_{i+2k+1,i+2k+3}^2 \right). \quad (3.16)$$

It is customary to subtract the one-loop finite part of the BDS amplitude A_{BDS} that was written down in [2]. Since both A_{BDS} and $A_{\text{BDS-like}}$ satisfy the same anomalous Ward identity of dual conformal invariance [65], their difference can only be a function of the conformal cross ratios introduced in section 2. For seven points this is written down in [66] and reads

$$\begin{aligned} \Delta := A_{\text{BDS-like}} - A_{\text{BDS}} = & -\frac{1}{4} \sum_{i=1}^7 (\log^2 u_i + \text{Li}_2(1 - u_i)) + \frac{1}{8} \log u_{11} \log \left(\frac{u_{21} u_{22}}{\tilde{u} u_{32}} \right) \\ & + \frac{1}{8} \log u_{12} \log \left(\frac{u_{32} u_{31}}{\tilde{u} u_{21}} \right) + \frac{1}{8} \log u_{21} \log \left(\frac{u_{11} u_{32}}{u_{12} u_{22}} \right) + \frac{1}{8} \log u_{22} \log \left(\frac{u_{11} \tilde{u}}{u_{21} u_{31}} \right) \\ & + \frac{1}{8} \log u_{31} \log \left(\frac{u_{12} \tilde{u}}{u_{22} u_{32}} \right) + \frac{1}{8} \log u_{32} \log \left(\frac{u_{12} u_{21}}{u_{11} u_{31}} \right) + \frac{1}{8} \log \tilde{u} \log \left(\frac{u_{22} u_{31}}{u_{11} u_{12}} \right). \end{aligned} \quad (3.17)$$

The last missing piece of the amplitude is A_{per} , which is a function of the auxiliary parameters m_s and ϕ_s and is given by

$$A_{\text{per}} = \frac{|m_1|^2}{2} + \frac{|m_2|^2}{2} + \frac{1}{\sqrt{2}} |m_1| |m_2| (\cos \phi_1 \cos \phi_2 + \sin \phi_1 \sin \phi_2) \quad (3.18)$$

for the 7-point amplitude. Once again, A_{per} becomes a function of the cross ratios once we understand how the system parameters are related to the kinematics, see next subsection. Summing things up, we can now write the remainder function R that was defined in Eq. (3.1) as

$$e^R := e^{-\frac{\sqrt{\Delta}}{2\pi}(\Delta + A_{\text{free}} + A_{\text{per}})} \quad (3.19)$$

This concludes our review of the remainder function in strongly coupled $\mathcal{N} = 4$ SYM theory. We can now begin to approach the multi-Regge regime.

3.2 Approaching multi-Regge kinematics

As we have stressed in the previous subsection the two terms A_{free} and A_{per} are still written as functions of the system parameters m_s, C_s and ϕ_s rather than the cross ratios $u_{a\sigma}$. Notice that the number $3n - 15$ of system parameters coincides with the number of independent cross ratios. Indeed, the two sets of variables can be mapped onto each other. As explained in [34], the cross ratios are connected to Y-functions evaluated at special values of the spectral parameter θ . More precisely, we have that

$$U_{ij} = \frac{Y_{2,i-j-2}^{[i+j+2]}}{1 + Y_{2,i-j-2}^{[i+j+2]}} \quad (3.20)$$

where $Y_{a,s}^{[k]}$ is shorthand for $Y_{a,s}^{[k]}(0) = Y_{a,s}(ik\frac{\pi}{4})$. Since the right-hand side depends only on the Y-system parameters, relation (3.20) can be inverted to determine their dependence on the cross ratios, i.e. on the kinematics of our scattering problem.

Imposing multi-Regge behavior for the cross ratios, we are driven to very special values of the Y-system parameters. Indeed, in [56] we find that the following limiting behavior of the system parameters

$$|m_s| \rightarrow \infty, \quad \phi_s \rightarrow (1-s)\frac{\pi}{4}, \quad C_s = \text{const.} \in i\mathbb{R} \quad (3.21)$$

leads to multi-Regge behavior as given in Eqs. (2.11) for the cross ratios. More specifically, introducing the parameters

$$\varepsilon_s = e^{-|m_s| \cos(\phi_s - (1-s)\frac{\pi}{4})}, \quad w_s = e^{|m_s| \sin(\phi_s - (1-s)\frac{\pi}{4})} \quad (3.22)$$

the cross ratios behave as

$$u_{1\sigma} = 1 - \varepsilon_{n-4-\sigma} \left(w_{n-4-\sigma} + \frac{1}{w_{n-4-\sigma}} + 2 \cosh C_{n-4-\sigma} \right), \quad (3.23)$$

$$u_{2\sigma} = \varepsilon_{n-4-\sigma} w_{n-4-\sigma}, \quad (3.24)$$

$$u_{3\sigma} = \frac{\varepsilon_{n-4-\sigma}}{w_{n-4-\sigma}}, \quad (3.25)$$

where the ε_s go to zero in the multi-Regge limit, while the w_s attain a constant value. These equations are valid up to higher corrections in the ε_s . The reason for this simplification is, again as shown in [56], that in the multi-Regge limit the integrals in Eqs. (3.4)-(3.6) can be neglected, although one possibly needs to pick up residue contributions, depending on the value of θ .

This is already enough information to calculate the remainder function in the multi-Regge regime before any cross ratio is analytically continued, i.e. in the Euclidean region. We know from [4, 5] that the remainder function must be trivial in this multi-Regge region and we show in appendix B that it is indeed the case. The triviality of the remainder function is closely related to that of the free energy. The latter has a beautiful physical interpretation. In the large mass limit, the quantum fluctuations in the auxiliary one-dimensional quantum system are suppressed. Hence the vacuum becomes trivial and so does the free energy. In the next subsection we shall explain how the one-dimensional quantum system manages to produce less trivial results for the other regions.

Before going there, let us briefly spell out the most important formulas of this subsection in the case of $n = 7$ since we need these expressions for our analysis in the final section. In this case, we have six Y-functions which determine the six independent cross ratios through

$$\begin{aligned} u_{11} &= \frac{Y_{2,2}^{[2]}}{1 + Y_{2,2}^{[2]}}, & u_{21} &= \frac{Y_{2,2}^{[-2]}}{1 + Y_{2,2}^{[-2]}}, & u_{31} &= \frac{Y_{2,2}^{[0]}}{1 + Y_{2,2}^{[0]}}, \\ u_{12} &= \frac{Y_{2,1}^{[-3]}}{1 + Y_{2,1}^{[-3]}}, & u_{22} &= \frac{Y_{2,1}^{[-1]}}{1 + Y_{2,1}^{[-1]}}, & u_{32} &= \frac{Y_{2,1}^{[1]}}{1 + Y_{2,1}^{[1]}}. \end{aligned} \quad (3.26)$$

The values of the Y-system parameters in the multi-Regge limit are given by

$$|m_s| \rightarrow \text{large}, \quad \phi_1 \rightarrow 0, \quad \phi_2 \rightarrow -i\frac{\pi}{4}, \quad C_s = \text{const.}, \quad (3.27)$$

and from Eqs. (3.23)-(3.25) we find the behavior of the cross ratios to take the form

$$\begin{aligned} u_{11} &= 1 - \left(w_2 + \frac{1}{w_2} + 2 \cosh C_2 \right) \varepsilon_2, & u_{21} &= w_2 \varepsilon_2, & u_{31} &= \frac{\varepsilon_2}{w_2}, \\ u_{12} &= 1 - \left(w_1 + \frac{1}{w_1} + 2 \cosh C_1 \right) \varepsilon_1, & u_{22} &= w_1 \varepsilon_1, & u_{32} &= \frac{\varepsilon_1}{w_1}. \end{aligned} \quad (3.28)$$

This is all the input we need for the computation of the remainder function in various Regge regions in section 4.

3.3 Amplitude and multi-Regge Bethe Ansatz

As mentioned in the previous subsection, the non-linear integral equations that control the n -gluon amplitude at strong coupling simplify drastically when we take the multi-Regge limit. In fact, in the limiting regime we can actually neglect the integral contributions. Such a limit is well known in the theory of integrable systems. It corresponds to an infrared limit in which the solution of the integrable model boils down to solving a set of algebraic Bethe Ansatz equations.

Before performing the multi-Regge limit, the Y-system for scattering amplitudes of strongly coupled $\mathcal{N} = 4$ SYM theory takes the general form

$$\log \tilde{Y}_{a,s}(\theta) = -p_{a,s}(\theta) + \sum_{a',s'} \int d\theta' K_{s,s'}^{a,a'}(\theta - \theta' + i\phi_s - i\phi_{s'}) \log \left(1 + \tilde{Y}_{a',s'}(\theta') \right). \quad (3.29)$$

The source terms $p_{a,s}$ and the kernels $K_{s,s'}^{a,a'}$ depend on the $3n - 15$ parameters $|m_s|, C_s$ and ϕ_s in a way that was spelled out in the previous subsection. The expressions for the source terms are easy to state,

$$p_{2,s}(\theta) = \sqrt{2}|m_s| \cosh \theta, \quad p_{2\pm 1,s}(\theta) = |m_s| \cosh \theta \mp C_s \quad (3.30)$$

and we leave it to the reader to infer formulas for the kernels from our discussion above. As we explained before, we can use Eqs. (3.29) as long as $|\phi_s - \phi_{s+1}| < \pi/4$. Once we have solved for the $\tilde{Y}_{a,s}$ we can compute the free energy through the formula Eq. (3.15). In all these formulas, integrations are performed over the real axis.

We are now prepared to review how Bethe Ansatz equations emerge from the Y-system. In order to do so, we represent the kernel functions $K_{s,s'}^{a,a'}$ through new objects $S_{s,s'}^{a,a'}$,

$$-2\pi i K_{s,s'}^{a,a'}(\theta) =: \partial_\theta \log S_{s,s'}^{a,a'}(\theta). \quad (3.31)$$

As specific examples, the S-matrices corresponding to the basic kernels Eq. (3.10) take the form

$$S_1(\theta) = i \frac{1 - ie^\theta}{1 + ie^\theta}, \quad S_2(\theta) = \frac{2i \sinh \theta - \sqrt{2}}{2i \sinh \theta + \sqrt{2}}, \quad S_3(\theta) = \cosh 2\theta. \quad (3.32)$$

As Dorey and Tateo [67, 68] observed in the context of one-dimensional integrable systems, the form of the Y-system equations can change as one deforms the system parameters. In fact, upon analytic continuation of the parameters $|m_s|, C_s$ and ϕ_s of the Y-system some of the solutions to the equations $\tilde{Y}_{a,s}(\theta) = -1$ may cross the real axis. We shall enumerate those solutions by an index ν

$$\tilde{Y}_{a,s}(\theta_\nu^{(a,s)}) = -1, \text{ for } \nu = 1, \dots, N_{a,s} \quad (3.33)$$

When this happens, the integral on the right-hand side of Eq. (3.29) picks up a residue term since there is a pole crossing the integration contour. Hence, after analytic continuation the equations (3.29) take the form

$$\log \tilde{Y}'_{a,s}(\theta) = -p'_{a,s}(\theta) + \sum_{a',s'} \sum_{\nu=1}^{N_{a',s'}} \mu_\nu^{(a',s')} \log S_{s,s'}^{a,a'}(\theta - \theta_\nu^{(a',s')} + i\phi'_s - i\phi'_{s'}) \quad (3.34)$$

$$+ \sum_{a',s'} \int d\theta' K_{s,s'}^{a,a'}(\theta - \theta' + i\phi'_s - i\phi'_{s'}) \log \left(1 + \tilde{Y}'_{a',s'}(\theta') \right). \quad (3.35)$$

Here, the sign factors $\mu_\nu^{(a,s)} \in \{\pm 1\}$ depend on whether the solution of Eq. (3.33) crosses from the lower into the upper half-plane or in the opposite direction. At the endpoint of the continuation, the system parameters assume the values $|m_s|', C'_s$ and ϕ'_s , which may differ from those we started with. Therefore, we place a prime on all quantities that are defined in terms of the system parameters. Later we shall impose the condition that our continuation corresponds to a specific curve in the space of cross ratios (cf. section 2.3). That allows us to determine the primed system parameters. Before we do so, let us now send the system parameters of our non-linear integral equations into a regime where the integrals can be neglected, e.g. into the

multi-Regge regime, where the Eqs. (3.35) become

$$\log \tilde{Y}'_{a,s}(\theta) = -p'_{a,s}(\theta) + \sum_{a',s'} \sum_{\nu=1}^{N_{a',s'}} \mu_{\nu}^{(a',s')} \log S_{s,s'}^{a,a'}(\theta - \theta_{\nu}^{(a',s')} + i\phi'_s - i\phi'_{s'}). \quad (3.36)$$

We can exponentiate this set of equations for the functions $\tilde{Y}'_{a,s}(\theta)$ and insert the values $\theta = \theta_{\nu}^{(a,s)}$ satisfying Eq. (3.33) to obtain

$$-e^{p'_{a,s}(\theta_{\mu}^{(a,s)})} = \prod_{a',s'} \prod_{\nu=1}^{N_{a',s'}} S_{s,s'}^{a,a'}(\theta_{\mu}^{(a,s)} - \theta_{\nu}^{(a',s')} + i\phi'_s - i\phi'_{s'})^{\mu_{\nu}^{(a',s')}}. \quad (3.37)$$

In our context, these equations simply determine the possible location of the solutions $\theta_{\nu}^{(a,s)}$ to Eqs. (3.33) and we will call them *endpoint conditions* in the following. The form of the equations coincides with a usual Bethe Ansatz which imposes single-valuedness of wave functions for a dilute system of particles on a one-dimensional circle of radius R . The term $e^{p'_{a,s}}$ accounts for the phase shift of a freely moving particle with momentum $k'_{a,s}(\theta_{\nu}^{(a,s)}) = -ip'_{a,s}(\theta_{\nu}^{(a,s)})/R$ when we take it once around a circle of radius R . The remaining factors arise from the scattering with other particles that may be distributed along the one-dimensional circle. Hence, the quantities $S_{s,s'}^{a,a'}$ introduced in Eq. (3.31) are interpreted as scattering matrices for excitations of some integrable system and the source terms $k'_{a,s}$ describe the momentum.

Once we have found a solution for the Eqs. (3.37), we can insert it back into the Eqs. (3.36) to determine the functions \tilde{Y} . From these \tilde{Y} -functions we then compute the cross ratios. This may require repeated use of the recursion relations (3.12) for the Y-functions, but it is straightforward. The resulting formulas express the cross ratios u_{as} through the primed system parameters and a solution of the Eqs. (3.37). We can solve these equations for the primed system parameters in terms of the parameters at the starting point of the continuation. Of course, the relation depends on the choice of a solution to the Bethe Ansatz Eqs. (3.37).

Let us finally discuss the form of the free energy (3.15). Upon analytic continuation of the parameters, the Y-functions may again give rise to pole terms that cross the real axis, because the integrand has the same structure as in the Y-system. This happens precisely when the conditions (3.33) are satisfied. After taking the multi-Regge limit, only these pole terms survive and we obtain an expression of the form

$$A'_{\text{free}} = - \sum_{a,s} \sum_{\nu=1}^{N_{a,s}} i(\sqrt{2})^{\delta_{a,2}} \mu_{\nu}^{(a,s)} |m_s|' \sinh(\theta_{\nu}^{(a,s)}). \quad (3.38)$$

Recall that the quantities m'_s and ϕ'_s are considered as functions of the cross ratios and the Bethe roots $\theta_{\nu}^{(a,s)}$, as described in the previous paragraph. Once the explicit expressions are plugged in, we can extract the leading terms in the multi Regge limit $|m_s|' \rightarrow \infty$. This completes our task to explain the role of the Bethe Ansatz (3.37) in the multi-Regge regime of strongly coupled $\mathcal{N} = 4$ SYM theory.

We have shown that upon analytic continuation of the cross ratios, and hence of the system parameters $|m_s|$, C_s and ϕ_s , the Y-system can pick up additional terms from residue contributions. These may be thought off as excitations above the ground state. As we approach the

multi-Regge regime, i.e. send the mass parameters m_s to infinity, the quantum fluctuations are suppressed, as explained before. In this limit, the free energy of the system is determined by the bare energies of the excitations that were produced during the continuation, as expressed in Eq. (3.38). In case no excitations appeared, the free energy would continue to vanish in the multi-Regge limit. We shall, however, see excitations for most of the regions we analyze below.

In order to conclude this section and warm up for the next, let us illustrate all the above for the example of $n = 6$ external gluons, see [55, 69]. Since for six gluons the parameter s is fixed to 1, we will suppress it in the following. In [55, 69], we start from a set of parameters $(|m|, C, \phi)$ with ϕ small and continue along a particular curve such that the cross ratio u_1 performs a full rotation, while the other cross ratios remain fixed, see path $P_{6,-}$ in subsection 2.3. At the endpoint of the continuation we reach another point $(|m'|, C', \phi')$ in the complexified parameter space corresponding to the same values of the cross ratios, i.e. $u_a(|m|, C, \phi) = u_a(|m'|, C', \phi')$. A numerical analysis of the Y-system equations shows that, along this path, two solutions of the equation $\tilde{Y}_3(\theta_*) = -1$ (or of $\tilde{Y}_1(\theta_*)$, depending on the value of C) cross the real axis while two solutions of $\tilde{Y}_2(\theta_*) = -1$ approach the real axis. The solution of $\tilde{Y}_3(\theta_*) = -1$ crossing into the positive (negative) half-plane will be called θ_+ (θ_-) in the following. For the 6-gluon case, there is a special symmetry of the Y-system,

$$\tilde{Y}_a(\theta) = \tilde{Y}_a(-\theta). \quad (3.39)$$

In [69] we show that due to this symmetry, the two solutions of \tilde{Y}_2 pinch the integration contour, but never cross and therefore do not contribute to the free energy term or the Y-system. We can then spell out the equations at the endpoint of the continuation,

$$\log \tilde{Y}_2(\theta) = -\sqrt{2}|m'| \cosh \theta + \log S_2(\theta - \theta_-) - \log S_2(\theta - \theta_+), \quad (3.40)$$

$$\log \tilde{Y}_{2\pm 1}(\theta) = -|m'| \cosh \theta \pm C' + \log S_1(\theta - \theta_-) - \log S_1(\theta - \theta_+). \quad (3.41)$$

Since there are two Bethe roots, the Bethe Ansatz consists of two equations. It turns out that these equations are identical due to the above-mentioned symmetry so that we end up with

$$-e^{p'_3(\theta_+)} = \frac{S_1(\theta_+ - \theta_-)}{S_1(0)}, \quad (3.42)$$

where $S_1(\theta)$ was spelled out in Eq. (3.32) and where $p'_3(\theta_+) = |m'| \cosh \theta_+$. Note that $\mu_-^{(3)} = -\mu_+^{(3)} = 1$. When we perform the multi-Regge limit $|m'| \rightarrow \infty$ in Eq. (3.42), the left hand side of our Bethe Ansatz equation diverges and hence $\theta_+ - \theta_-$ has to approach a pole of S_1 . Hence, because of the pole structure of $S_1(\theta)$, our solution consists of one Bethe string with

$$\theta_+ - \theta_- = i\frac{\pi}{2}. \quad (3.43)$$

Furthermore, taking into account the symmetry Eq. (3.39) which relates the endpoints θ_{\pm} as

$$\theta_- = -\theta_+ \quad (3.44)$$

we can conclude that the endpoints of the crossed solutions are at

$$\theta_{\pm} = \pm i\frac{\pi}{4}. \quad (3.45)$$

Using Eqs. (3.40),(3.41) together with the recursion relations, we obtain the cross ratios

$$u'_1 = 1 - \gamma \varepsilon' \left(w' + \frac{1}{w'} - 2 \cosh C' \right), \quad (3.46)$$

$$u'_2 = \gamma w' \varepsilon', \quad (3.47)$$

$$u'_3 = \gamma \frac{\varepsilon'}{w'}, \quad (3.48)$$

with $\gamma = -(3 + 2\sqrt{2})$ and the parameters w', ε' are related to the primed parameters through Eqs. (3.22). The above expressions are valid up to corrections of $\mathcal{O}(\varepsilon'^2)$. Imposing $u_a = u'_a$ we obtain relations between the primed and the unprimed parameters and find

$$\varepsilon' = \frac{1}{\gamma} \varepsilon, \quad w' = w, \quad \cosh C' = -\cosh C, \quad (3.49)$$

again up to subleading corrections. Now we can compute the free energy in terms of the primed parameters through Eq. (3.38) and then express the primed parameters through the original ones to find

$$A'_{\text{free}}{}^{(6)} = \sqrt{2} \log \varepsilon - \sqrt{2} \log \gamma + \mathcal{O}(\varepsilon \log \varepsilon). \quad (3.50)$$

This ends our example, for more details on the calculation see [69]. We can perform a similar analysis for any solution of the Bethe Ansatz Eq. (3.37) and will do so for the 7-point amplitude in the next section.

4 Results for the 7-point amplitude

We now turn to the explicit calculation of the remainder function in various Regge regions of the 7-point amplitude. The kinematics and the various non-trivial multi-Regge regions for this amplitude were described in section 3.2. In principle it is not difficult to follow our general algorithm for the calculation of the remainder function at strong coupling. We know that each region corresponds to a particular pattern of Bethe roots. Once these are determined as a solution of Eqs. (3.37), calculating the remainder function is a bit cumbersome, but straightforward. The main issue is to associate a solution of Eq. (3.37) with each of the four non-trivial multi-Regge regions that exist for $n = 7$. So far, the only way we can make this association is through a numerical analysis of the Y-system. Once we have understood which solutions of the Eqs. (3.33) cross the real axis, the relevant solution and the amplitude can be computed analytically.

For the numerical investigations it is advantageous to reformulate the original Y-system such that the driving terms contain the cross ratios rather than the system parameters m_s, C_s and ϕ_s . This will be explained in the first subsection. Then we discuss each of the four non-trivial multi-Regge regions, starting with the region $(- - +)$. In each case we present our numerical results before we apply the insights they provide to calculate the remainder functions. We also compare the final expressions for the remainder functions with the expectations from weak coupling.

4.1 An alternative Y-system

As described in the general algorithm in section 3.3, a crucial part of the calculation is to follow the solutions of the equations

$$\tilde{Y}_{a,s}(\theta) = -1 \quad (4.1)$$

through the θ -plane as we analytically continue the cross ratios. At the moment we can only do this through numerical studies of the Y-system. But with the Y-system (3.4)-(3.6) this is a rather difficult task as we would first need to determine how the auxiliary parameters $|m_s|$, C_s and ϕ_s behave along the path of continuation. In order to circumvent the issue, we shall pass to a different version of the Y-system, similar to the one derived in appendix F of [43].

Note that our choice of cross ratios can be obtained via the recursion relations if we know the following special values of Y-functions

$$\tilde{Y}_{1,1}(0), \tilde{Y}_{2,1}\left(-i\frac{\pi}{4}\right), \tilde{Y}_{3,1}(0), \tilde{Y}_{1,2}(0), \tilde{Y}_{2,2}\left(i\frac{\pi}{4}\right), \tilde{Y}_{3,2}(0), \quad (4.2)$$

Here, all arguments lie in the fundamental strip $|\operatorname{Im}\theta| \leq \frac{\pi}{4}$. In deriving concrete expressions one must use our choice of phases Eq. (3.21) to relate cross ratios defined in terms of Y-functions to the \tilde{Y} -functions. Since we prescribe the behavior of the cross ratios, we can use the recursion relations to infer the behavior of the values listed in Eq. (4.2) during the analytic continuation. Consequently, these values of our Y-functions are better suited as parameters in the Y-system equations than the auxiliary parameters $|m_s|$, C_s and ϕ_s . In order to work out the relevant equations, we solve the Y-system equations at the specific values of the spectral parameter θ that appear in Eq. (4.2) for the auxiliary parameters to obtain

$$\begin{aligned} C_s &= \frac{1}{2} \log \left(\frac{\tilde{Y}_{3,s}(0)}{\tilde{Y}_{1,s}(0)} \right) - \frac{1}{2} K_3 \star \gamma_s \Big|_{\theta=0}, \\ |m_s| &= -\frac{1}{2} \log \left(\tilde{Y}_{1,s}(0) \tilde{Y}_{3,s}(0) \right) - \frac{1}{2} K_2 \star \beta_s \Big|_{\theta=0} - K_1 \star \alpha_s \Big|_{\theta=0}. \end{aligned} \quad (4.3)$$

Note that none of the $\tilde{Y}_{2,s}$ variables appears in Eqs. (4.3). The reason for this is that we are working with fixed phases for simplicity and therefore do not replace the parameters ϕ_s in the original equations⁴. We can now plug Eqs. (4.3) in the original Y-system equations and obtain

⁴Note that for some of the paths describes in section 3.2 we have a relative rotation of small cross ratios which entails that we cannot keep the phases ϕ_s fixed during the continuation. However, we can estimate the size of the error by adding a small deviation from the fixed value, $\phi_s = (1-s)\frac{\pi}{4} + \epsilon_\phi$. Then, a relative rotation of $\pm 2i\varphi$ would entail

$$\frac{u_{2s}}{u_{3s}} = w_s^2 = e^{2|m_s| \sin(\phi_s - (1-s)\frac{\pi}{4})} = e^{2|m_s| \epsilon_\phi} \stackrel{!}{=} e^{\pm 2i\varphi}, \quad (4.4)$$

which gives

$$\epsilon_\phi = \frac{\pm i\varphi}{|m_s|} \sim \mathcal{O}\left(\frac{1}{\log \varepsilon_s}\right) \quad (4.5)$$

and is therefore negligible throughout the continuation.

the new Y-system

$$\begin{aligned} \log \tilde{Y}_{1,s}(\theta) &= \frac{1}{2} \log \left(\tilde{Y}_{1,s}(0) \tilde{Y}_{3,s}(0) \right) \cosh \theta - \frac{1}{2} \log \left(\frac{\tilde{Y}_{3,s}(0)}{\tilde{Y}_{1,s}(0)} \right) \\ &\quad + \sum_{a',s'} \int d\theta' \mathcal{K}_{s,s'}^{1,a'}(\theta, \theta') \log \left(1 + \tilde{Y}_{a',s'}(\theta') \right), \end{aligned} \quad (4.6)$$

$$\log \tilde{Y}_{2,s}(\theta) = \frac{1}{\sqrt{2}} \log \left(\tilde{Y}_{1,s}(0) \tilde{Y}_{3,s}(0) \right) \cosh \theta + \sum_{a',s'} \int d\theta' \mathcal{K}_{s,s'}^{2,a'}(\theta, \theta') \log \left(1 + \tilde{Y}_{a',s'}(\theta') \right), \quad (4.7)$$

$$\begin{aligned} \log \tilde{Y}_{3,s}(\theta) &= \frac{1}{2} \log \left(\tilde{Y}_{1,s}(0) \tilde{Y}_{3,s}(0) \right) \cosh \theta + \frac{1}{2} \log \left(\frac{\tilde{Y}_{3,s}(0)}{\tilde{Y}_{1,s}(0)} \right) \\ &\quad + \sum_{a',s'} \int d\theta' \mathcal{K}_{s,s'}^{3,a'}(\theta, \theta') \log \left(1 + \tilde{Y}_{a',s'}(\theta') \right). \end{aligned} \quad (4.8)$$

The new kernels are more complicated compared to the kernels of the original Y-system and are spelled out in appendix C.

4.2 Remainder function in the Regge region $(- - +)$

We now evaluate the remainder function in the first relevant Regge region, namely the region $(- - +)$, which we probe via the path $P_{7,- - +}$ that was defined in Eq. (2.24). Prescribing this behavior of the cross ratios, we solve the recursion relations for the driving terms of the modified Y-system Eqs. (4.6)-(4.8) numerically. We find the results shown in figure 3.

4.2.1 Numerical analysis of the continuation

After finding the paths of continuation for the driving terms, we now turn to the determination of A_{free} . To do so, we need to determine those $\tilde{Y}_{a,s}$ -functions for which a solution to the equation $\tilde{Y}_{a,s} = -1$ crosses the real axis, as explained in detail in section 3.3. Since we know the behavior of the system parameters in the new Y-system along the path of continuation, we can simply solve the Y-system in the complex θ -plane for each value of φ and then determine the location of the solutions $\tilde{Y}_{a,s} = -1$. We solve the Y-system by an iterative procedure, similar to the algorithm presented in [34].

Following this procedure, we find the behavior for the \tilde{Y} -functions displayed in figure 4. We see that a pair of solutions of $\tilde{Y}_{3,2}$ crosses the real axis and approaches the values $\pm i\frac{\pi}{4}$ at the end of the continuation. Furthermore, two solutions of $\tilde{Y}_{2,2}$ approach the origin at the end of the continuation. As we show in the next section, the Y-system equations for the triplet $\tilde{Y}_{a,2}$ at the end of the continuation are of the same form as the equations for the 6-point case in section 3.3. Therefore, we can argue as in the 6-point case that the pair of solutions of $\tilde{Y}_{2,2}$ never crosses the integration contour and we just have to consider the pair of crossing solutions of $\tilde{Y}_{3,2}(\theta)$. Furthermore, since we find the same equations as in the 6-point case for the triplet $\tilde{Y}_{a,2}$, we can use the endpoint conditions Eq.(3.37) to analytically determine the endpoint of the Bethe roots to be $\pm i\frac{\pi}{4}$, confirming our numerical analysis.

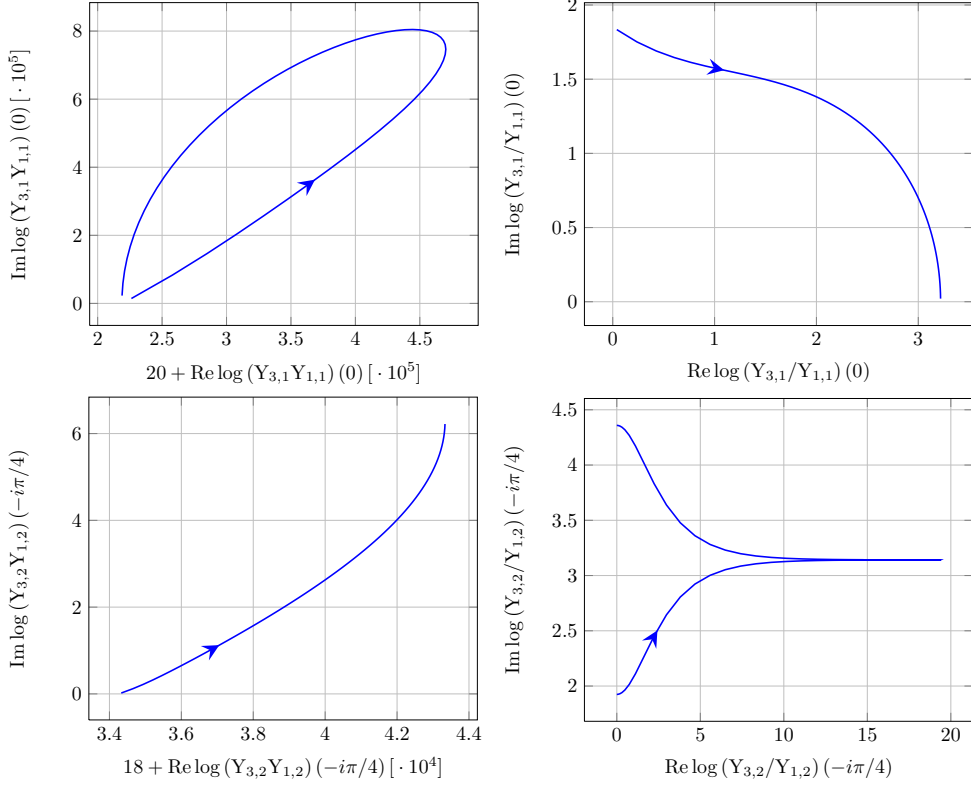


Figure 3. Paths of the driving terms during the analytic continuation for the path Eq. (2.24). The starting values for the parameters chosen here are $|m_1| = 10$, $|m_2| = 9$, $C_1 = \operatorname{arccosh}(\frac{3}{5})$, $C_2 = \operatorname{arccosh}(\frac{4}{7})$. Note that some axes have been shifted and rescaled. The direction of growing φ is indicated by the arrows.

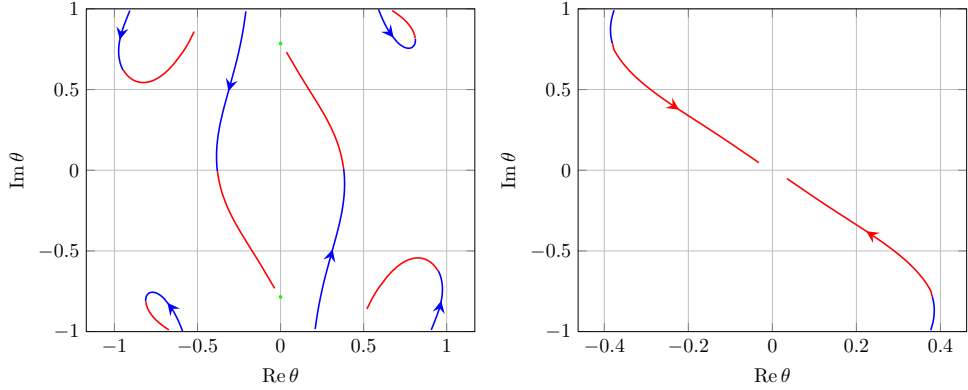


Figure 4. Left: Crossing solutions of $\tilde{Y}_{3,2}(\theta) = -1$ during the continuation Eq. (2.24). We find that two solutions cross the real axis and approach the endpoints $\pm i\frac{\pi}{4}$. Right: Towards the end of the continuation, a pair of solutions of $\tilde{Y}_{2,2}(\theta) = -1$ approaches the real axis, but does not contribute to the remainder function as is argued in the main text. The direction of growing φ is indicated by the arrows.

4.2.2 Calculation of the remainder function

Using the input from the numerical analysis, we can now determine the amplitude. Let us stress again that the input from the numerics is discrete - it only provides information on which Y-functions have crossed. The endpoints can be determined analytically, therefore our result derived below is not bound to any numerical accuracy. Note also that since we are done with the numerical analysis, we can switch back to the standard Y-system Eqs. (3.4)-(3.6), because the crossing solutions of the \tilde{Y} -functions are independent of the choice of system parameters, of course. As a first step, let us determine the cross ratios at the end of the continuation. In the following, all quantities that have been analytically continued are marked with a prime, as before. At the end of the continuation, the Y-system takes the following form:

$$\begin{aligned} \log \tilde{Y}'_{1,s} &= -|m_s|' \cosh \theta - C'_s + \sum_{a',s'} \int d\theta' K_{s,s'}^{1,a'} (\theta - \theta' + i\phi'_s - i\phi'_{s'}) \log \left(1 + \tilde{Y}'_{a',s'}(\theta') \right) \\ &+ \log \frac{S_{s,2}^{1,3}(\theta + i\frac{\pi}{4} + i\phi'_s - i\phi'_2)}{S_{s,2}^{1,3}(\theta - i\frac{\pi}{4} + i\phi'_s - i\phi'_2)}, \end{aligned} \quad (4.9)$$

$$\begin{aligned} \log \tilde{Y}'_{2,s} &= -\sqrt{2}|m_s|' \cosh \theta + \sum_{a',s'} \int d\theta' K_{s,s'}^{2,a'} (\theta - \theta' + i\phi'_s - i\phi'_{s'}) \log \left(1 + \tilde{Y}'_{a',s'}(\theta') \right) \\ &+ \log \frac{S_{s,2}^{2,3}(\theta + i\frac{\pi}{4} + i\phi'_s - i\phi'_2)}{S_{s,2}^{2,3}(\theta - i\frac{\pi}{4} + i\phi'_s - i\phi'_2)}, \end{aligned} \quad (4.10)$$

$$\begin{aligned} \log \tilde{Y}'_{3,s} &= -|m_s|' \cosh \theta + C'_s + \sum_{a',s'} \int d\theta' K_{s,s'}^{3,a'} (\theta - \theta' + i\phi'_s - i\phi'_{s'}) \log \left(1 + \tilde{Y}'_{a',s'}(\theta') \right) \\ &+ \log \frac{S_{s,2}^{3,3}(\theta + i\frac{\pi}{4} + i\phi'_s - i\phi'_2)}{S_{s,2}^{3,3}(\theta - i\frac{\pi}{4} + i\phi'_s - i\phi'_2)}. \end{aligned} \quad (4.11)$$

As we now go to the multi-Regge limit, we can neglect the integrals and are left with the equations

$$Y'_{1,s} = \left(e^{-|m_s|' \cosh(\theta - i\phi'_s) - C'_s} \right) \frac{S_{s,2}^{1,3}(\theta + i\frac{\pi}{4} - i\phi'_2)}{S_{s,2}^{1,3}(\theta - i\frac{\pi}{4} - i\phi'_2)}, \quad (4.12)$$

$$Y'_{2,s} = \left(e^{-\sqrt{2}|m_s|' \cosh(\theta - i\phi'_s)} \right) \frac{S_{s,2}^{2,3}(\theta + i\frac{\pi}{4} - i\phi'_2)}{S_{s,2}^{2,3}(\theta - i\frac{\pi}{4} - i\phi'_2)}, \quad (4.13)$$

$$Y'_{3,s} = \left(e^{-|m_s|' \cosh(\theta - i\phi'_s) + C'_s} \right) \frac{S_{s,2}^{3,3}(\theta + i\frac{\pi}{4} - i\phi'_2)}{S_{s,2}^{3,3}(\theta - i\frac{\pi}{4} - i\phi'_2)}. \quad (4.14)$$

Using the recursion relations and introducing the parameters

$$\varepsilon' := e^{-|m_s|' \cos((s-1)\frac{\pi}{4} + \phi'_s)}, \quad w' := e^{|m_s|' \sin((s-1)\frac{\pi}{4} + \phi'_s)}, \quad (4.15)$$

we find that the cross ratios at the end of the path are given by⁵

$$\begin{aligned} u'_{11} &= 1 - \gamma \varepsilon'_2 \left(w'_2 + \frac{1}{w'_2} - 2 \cosh C'_2 \right), & u'_{21} &= \gamma w'_2 \varepsilon'_2, & u'_{31} &= \gamma \frac{\varepsilon'_2}{w'_2}, \\ u'_{12} &= 1 + \varepsilon'_1 \left(\frac{1}{\gamma} w'_1 + \frac{1}{w'_1} + \frac{2}{\sqrt{-\gamma}} \sinh C'_1 \right), & u'_{22} &= -\frac{1}{\gamma} w'_1 \varepsilon'_1, & u'_{32} &= -\frac{\varepsilon'_1}{w'_1}, \end{aligned} \quad (4.16)$$

where $\gamma = -3 - 2\sqrt{2}$, and all above expressions are valid up to corrections of $\mathcal{O}(\varepsilon'^2)$. For the path under consideration we then impose $u'_{22} = -u_{22}$, $u'_{32} = -u_{32}$, as well as $u'_{as} = u_{as}$ for all other cross ratios. This determines ε'_s , w'_s and C'_s in terms of the old parameters, giving rise to the relations

$$\begin{aligned} \varepsilon'_1 &= \sqrt{\gamma} \varepsilon_1, & w'_1 &= \sqrt{\gamma} w_1, & \cosh C'_1 &= \sqrt{1 - (w_1 + w_1^{-1} + \cosh C_1)^2}, \\ \varepsilon'_2 &= \frac{1}{\gamma} \varepsilon_2, & w'_2 &= w_2, & \cosh C'_2 &= -\cosh C_2, \end{aligned} \quad (4.17)$$

again up to corrections $\mathcal{O}(\varepsilon^2)$. We can now examine the terms of the remainder function Eq. (3.19) after the continuation piece by piece and see how they contribute. We start with A_{per} , which after the continuation reads

$$\begin{aligned} A'_{\text{per}} &= \frac{1}{2} \left(\log^2 \varepsilon'_1 + \log^2 w'_1 + \log^2 \varepsilon'_2 + \log^2 w'_2 \right. \\ &\quad \left. + \log \varepsilon'_1 \log \varepsilon'_2 + \log w'_1 \log w'_2 + \log \varepsilon'_2 \log w'_1 - \log \varepsilon'_1 \log w'_2 \right). \end{aligned} \quad (4.18)$$

Using Eq. (4.17), this gives

$$A'_{\text{per}} = A_{\text{per}} + \frac{1}{4} \log^2 \gamma - \frac{1}{2} \log \gamma \log \varepsilon_2. \quad (4.19)$$

We next turn to A_{free} . We determined the relevant crossings already in the last section. Furthermore, we know from section 3.3 that in the multi Regge-limit only the residue terms from the crossing \tilde{Y} -functions contribute to the free energy. In the last section we saw that one pair of solutions of $\tilde{Y}_{3,2}$ crosses the real axis and approaches the endpoints $\pm i\frac{\pi}{4}$. After neglecting the integrals, we are therefore left with

$$\begin{aligned} A'_{\text{free}} &= -\frac{|m_2|}{2\pi} \left(2\pi i \sinh\left(-i\frac{\pi}{4}\right) - 2\pi i \sinh\left(i\frac{\pi}{4}\right) \right) \\ &= -\sqrt{2} \sqrt{\log^2 \varepsilon'_2 + \log^2 w'_2} \\ &\approx +\sqrt{2} \log \varepsilon'_2 = +\sqrt{2} (\log \varepsilon_2 - \log \gamma). \end{aligned} \quad (4.20)$$

This leaves us with Δ' , whose form before continuation was spelled out in Eq. (3.17). During the continuation, some cut contributions have to be picked up and we end up with

$$\begin{aligned} \Delta' &= \Delta - i\frac{\pi}{4} (2 \log u_{11} + \log u_{12} + \log \tilde{u} - 2 \log(1 - u_{11})) \\ &\quad + \frac{1}{4} (\text{Li}_2(1 - u_{22}) - \text{Li}_2(1 + u_{22}) + \text{Li}_2(1 - u_{32}) - \text{Li}_2(1 + u_{32})) + \text{const.} \\ &= -i\frac{\pi}{2} \log \varepsilon_2 - i\frac{\pi}{2} \log (w_2 + w_2^{-1} + 2 \cosh C_2) + \text{const.} + \mathcal{O}(\varepsilon). \end{aligned} \quad (4.21)$$

⁵Note that in evaluating the cross ratios we set $\phi'_s = \phi_s$ in the S-matrix factors. The error we are making with this choice is of the same order as in Eq. (4.5) and therefore negligible.

Adding all contributions and using⁶ $\log \gamma = \log |\gamma| - i\pi$ we find

$$A'_{\text{per}} + A'_{\text{free}} + \Delta' + i\delta'_{7,--+} = -e_2 \log \varepsilon_2 - i\pi e_2 + \text{const.} + \mathcal{O}(\varepsilon), \quad (4.22)$$

where

$$e_2 = -\sqrt{2} + \log(1 + \sqrt{2}) \quad (4.23)$$

and where

$$\delta'_{7,--+} = \frac{\pi}{2} \log \left(w_2 + \frac{1}{w_2} + 2 \cosh C_2 \right) \quad (4.24)$$

is a phase that cancels with an equivalent term in the BDS-part in the full amplitude. To rewrite this result in terms of the cross ratios we use the relations

$$\varepsilon_2 = \sqrt{\tilde{u}_{21}\tilde{u}_{31}}(1 - u_{11}), \quad w_2 = \sqrt{\frac{u_{21}}{u_{31}}} \quad (4.25)$$

and obtain

$$A'_{\text{per}} + A'_{\text{free}} + \Delta' + i\delta'_{7,--+} = \frac{\sqrt{\lambda}}{2\pi} (e_2 \log(-(1 - u_{11})\tilde{u}_{21}\tilde{u}_{31}) + \text{const.}). \quad (4.26)$$

Exponentiating, we obtain our final result for the remainder function

$$e^{R_{7,--+} + i\delta_{7,--+}} \Big|_{\text{MRL}} \sim \left(-(1 - u_{11})\sqrt{\tilde{u}_{21}\tilde{u}_{31}} \right)^{\frac{\sqrt{\lambda}}{2\pi} e_2}, \quad (4.27)$$

where

$$\delta_{7,--+} = \frac{\sqrt{\lambda}}{2} \log(\tilde{u}_{21}\tilde{u}_{31}) = \frac{\pi}{2} \gamma_K \log(\tilde{u}_{21}\tilde{u}_{31}) \quad (4.28)$$

with the strong coupling limit of the cusp anomalous dimension $\gamma_K = \frac{\sqrt{\lambda}}{\pi}$. Remarkably, this result can be expressed in the same form as the 6-point result, $R_{7,--+}(u_{as}) = R_{6,--}(u_{11}, u_{21}, u_{31})$, and nicely matches the weak-coupling predictions as stated in section 2.4.

Note that in this section we have focused on the calculation for the region $P_{7,--+}$. The calculation for the region $P_{7,+--}$ is very similar and is therefore presented in appendix E. Here we only present the final result, which reads

$$e^{R_{7,+--} + i\delta_{7,+--}} \sim \left(-(1 - u_{12})\sqrt{\tilde{u}_{22}\tilde{u}_{32}} \right)^{\frac{\sqrt{\lambda}}{2\pi} e_2}, \quad (4.29)$$

with

$$\delta_{7,+--} = \frac{\pi}{2} \gamma_K \log(\tilde{u}_{22}\tilde{u}_{32}) \quad (4.30)$$

showing manifestly the target-projectile symmetry Eq. (2.8) we have mentioned before.

⁶One way of fixing the ambiguity of the imaginary part of $\log \gamma$ is to calculate the original Y-system parameter $|m_s|$ numerically via Eq. (4.3) during the continuation. Comparing the numerical value at the endpoint with the analytic value for $|m_s|'$ obtained from Eq. (4.17) fixes $\log \gamma$.

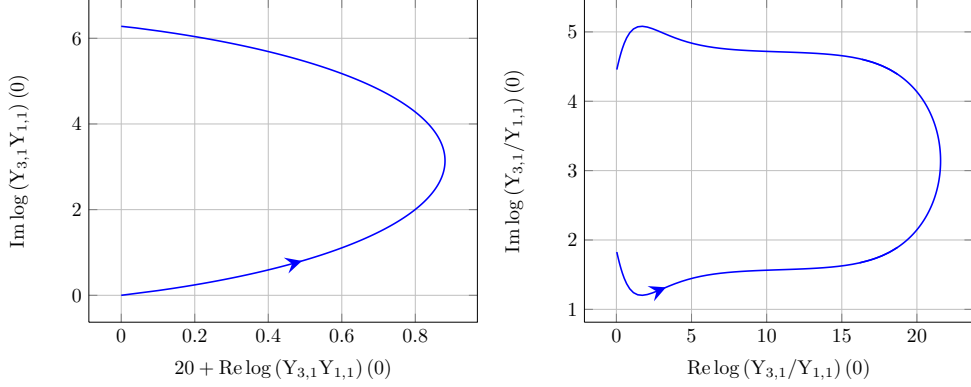


Figure 5. Solution of the driving terms during the continuation Eq. (2.25). The direction of growing φ is indicated by the arrows. For simplicity, the sets of parameters are identified as $|m| = |m_1| = |m_2| = 10$, $C = C_1 = -C_2 = \operatorname{arccosh}\left(\frac{3}{5}\right)$ at the starting point.

4.3 Remainder function in the Regge region (---)

After having discussed the paths with only two flipped legs, we now turn to the path where all produced particles are chosen to be incoming. As explained in section 2, the naive continuation along (semi-)circles fails for this path as it does not satisfy the conformal Gram relation. An appropriate deformation that is consistent with the Gram relation was spelled out in Eq. (2.25) and this is the one we will be using throughout our analysis. As before, we use the recursion relations to determine the behavior of the driving terms of the modified Y-system Eqs. (4.6)-(4.8). A plot of the curves followed by the driving terms during the continuation is shown in figure 5.

4.3.1 Numerical analysis of the continuation

We then turn to the numerical analysis of A_{free} for this Regge region. For the first time, we find that four solutions $\tilde{Y}_{a,s}(\theta) = -1$ from two different Y-functions, namely $\tilde{Y}_{3,1}$ and $\tilde{Y}_{1,2}$, cross the real axis. The endpoints of these crossing solutions will be called $\theta_{12\pm}$ and $\theta_{31\pm}$, respectively. The corresponding crossing plots are shown in figure 6. From figure 6 it is obvious that difference of the two pairs of crossed Bethe roots is given by $i\frac{\pi}{2}$. However, their absolute position does not seem to be a special point in the θ -plane. This is due to the relatively poor numerical convergence of the Y-functions for this particular path. In fact, while for all other paths studied so far mass parameters of the size of $\mathcal{O}(10)$ were enough to produce convergent Y-functions after only one iteration of the integral kernels, this is no longer true for this path. Therefore, the endpoints not ending on a distinguished point in the θ -plane is a reflection of the fact that we are not close enough to the limit $|m_s| \rightarrow \infty$ yet. Indeed, if we study the endpoint position of the Bethe roots as a function of the initial mass parameter we find the results shown in figure 7 as we increase the initial mass parameters towards infinity. The result of the numerical analysis then is that we have four crossing Bethe roots, two ending at $+i\frac{\pi}{4}$ and two ending at $-i\frac{\pi}{4}$. This numerical result can be backed up by analytical considerations as for the other paths. We begin by writing out the Y-system equations at the endpoint of the

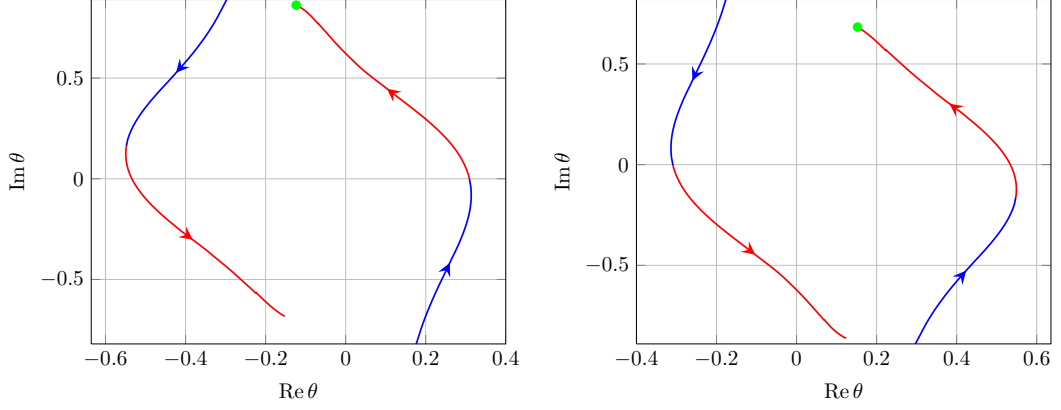


Figure 6. Crossing solutions of the functions $\tilde{Y}_{1,2}(\theta)$ (left) and $\tilde{Y}_{3,1}(\theta)$ (right) during the continuation Eq. (2.25). The mirror symmetry $\tilde{Y}_{1,2}(\theta) = \tilde{Y}_{3,1}(-\theta)$ is due to our choice $|m_1| = |m_2| = 10$, $C_1 = -C_2 = \text{arccosh}(\frac{3}{5})$ at the beginning of the continuation. The arrows indicate the direction of growing φ . We change colors once the first solution crosses the real axis.

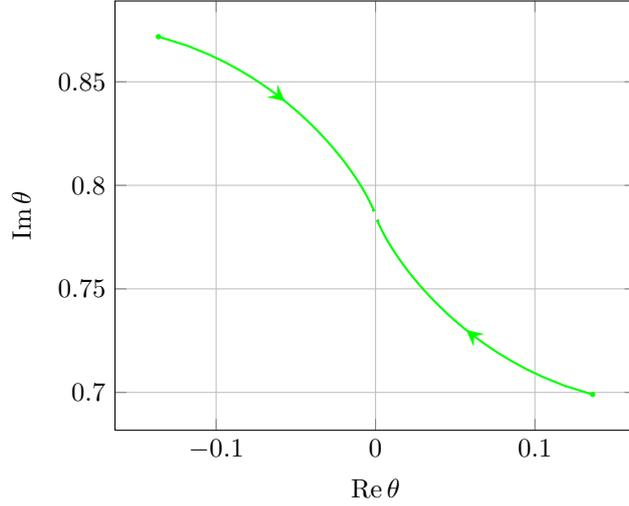


Figure 7. Convergence of the crossing solutions θ_{12+} and θ_{31+} against $i\frac{\pi}{4}$. The green dots indicate the position of the green dots in figure 6 and correspond to an initial value for the mass parameter of $|m_1| = |m_2| = 10$. We then increase the initial mass parameter up to $|m_1| = |m_2| = 2000$ until the convergence against $i\frac{\pi}{4}$ becomes obvious.

continuation:

$$\begin{aligned} \log \tilde{Y}'_{1,s}(\theta) &= -|m_s|' \cosh \theta - C'_s + \sum_{a',s'} \int d\theta' K_{s,s'}^{1,a'}(\theta - \theta' + i\phi'_s - i\phi'_{s'}) \log \left(1 + \tilde{Y}'_{a',s'}(\theta') \right) \\ &+ \log \frac{S_{s,2}^{1,1}(\theta - \theta_{12-} + i\phi'_s - i\phi'_2) S_{s,1}^{1,3}(\theta - \theta_{31-} + i\phi'_s - i\phi'_1)}{S_{s,2}^{1,1}(\theta - \theta_{12+} + i\phi'_s - i\phi'_2) S_{s,1}^{1,3}(\theta - \theta_{31+} + i\phi'_s - i\phi'_1)}, \end{aligned} \quad (4.31)$$

$$\begin{aligned} \log \tilde{Y}'_{2,s}(\theta) &= -\sqrt{2}|m_s|' \cosh \theta + \sum_{a',s'} \int d\theta' K_{s,s'}^{2,a'}(\theta - \theta' + i\phi'_s - i\phi'_{s'}) \log \left(1 + \tilde{Y}'_{a',s'}(\theta') \right) \\ &+ \log \frac{S_{s,2}^{2,1}(\theta - \theta_{12-} + i\phi'_s - i\phi'_2) S_{s,1}^{2,3}(\theta - \theta_{31-} + i\phi'_s - i\phi'_1)}{S_{s,2}^{2,1}(\theta - \theta_{12+} + i\phi'_s - i\phi'_2) S_{s,1}^{2,3}(\theta - \theta_{31+} + i\phi'_s - i\phi'_1)}, \end{aligned} \quad (4.32)$$

$$\begin{aligned} \log \tilde{Y}'_{3,s}(\theta) &= -|m_s|' \cosh \theta + C'_s + \sum_{a',s'} \int d\theta' K_{s,s'}^{3,a'}(\theta - \theta' + i\phi'_s - i\phi'_{s'}) \log \left(1 + \tilde{Y}'_{a',s'}(\theta') \right) \\ &+ \log \frac{S_{s,2}^{3,1}(\theta - \theta_{12-} + i\phi'_s - i\phi'_2) S_{s,1}^{3,3}(\theta - \theta_{31-} + i\phi'_s - i\phi'_1)}{S_{s,2}^{3,1}(\theta - \theta_{12+} + i\phi'_s - i\phi'_2) S_{s,1}^{3,3}(\theta - \theta_{31+} + i\phi'_s - i\phi'_1)}. \end{aligned} \quad (4.33)$$

From the standard two standard endpoint conditions $-1 = \tilde{Y}'_{1,2}(\theta_{12\pm}) = \tilde{Y}'_{3,1}(\theta_{31\pm})$, we only learn that

$$\theta_{12+} - \theta_{12-} = i\frac{\pi}{2} \quad \text{and} \quad \theta_{31+} - \theta_{31-} = i\frac{\pi}{2}. \quad (4.34)$$

However, we can also take into account the finiteness of ratios of Y-functions at the endpoint of the continuation,

$$\begin{aligned} 1 &= \frac{\tilde{Y}'_{1,2}(\theta_{12-})}{\tilde{Y}'_{1,2}(\theta_{12+})} = -e^{|m_2|'(\cosh \theta_{12+} + i \sinh \theta_{12+})} \left(\frac{1 + \cosh(\theta_{12+} - \theta_{31+}) + i \sinh(\theta_{12+} - \theta_{31+})}{1 - \cosh(\theta_{12+} - \theta_{31+}) - i \sinh(\theta_{12+} - \theta_{31+})} \right) \\ &= \frac{\tilde{Y}'_{3,1}(\theta_{31-})}{\tilde{Y}'_{3,1}(\theta_{31+})} = -e^{|m_1|'(\cosh \theta_{31+} + i \sinh \theta_{31+})} \left(\frac{1 - \cosh(\theta_{12+} - \theta_{31+}) - i \sinh(\theta_{12+} - \theta_{31+})}{1 + \cosh(\theta_{12+} - \theta_{31+}) + i \sinh(\theta_{12+} - \theta_{31+})} \right), \end{aligned} \quad (4.35)$$

where we have already used Eq. (4.34). As before, the S-matrix factors have to either diverge or go to zero as we send the mass parameters to infinity to give a finite product, depending on the sign of the exponent. However, we see that in Eq. (4.35) the S-matrix factors of the two equations are inverses of each other. Therefore, one of the S-matrix factors has to go to zero, while the other diverges. This is satisfied if

$$\theta_{12+} = \theta_{31+}. \quad (4.36)$$

This leaves us with one undetermined endpoint. Taking the product of the two equations (4.35) and using Eq. (4.36),

$$1 = e^{(|m_1|' + |m_2|')(\cosh \theta_{12+} + i \sinh \theta_{12+})}, \quad (4.37)$$

we see that the driving term has to be zero which finally gives us $\theta_{12+} = \theta_{31+} = i\frac{\pi}{4}$. Although certainly more complicated than in the other cases studied so far, this is a very pleasing result, as it reinforces our belief that we only need discrete input from the numerical calculations and can calculate the endpoints analytically.

4.3.2 Calculation of the remainder function

We now have all the necessary information to calculate the remainder function $R_{7,----}$. As the calculation is similar to the one presented in section 4.2, we will be brief. First, we calculate the cross ratios from Eqs. (4.31)-(4.33) and obtain

$$\begin{aligned} u'_{11} &= 1 + \varepsilon'_2 \left(\frac{1}{w'_2} + \gamma w'_2 + 2\sqrt{-\gamma} \sinh C'_2 \right), & u'_{21} &= -\gamma w'_2 \varepsilon'_2, & u'_{31} &= -\frac{\varepsilon'_2}{w'_2}, \\ u'_{12} &= 1 + \varepsilon'_1 \left(w'_1 + \frac{\gamma}{w'_1} + 2\sqrt{-\gamma} \sinh C'_1 \right), & u'_{22} &= -w'_1 \varepsilon'_1, & u'_{31} &= -\gamma \frac{\varepsilon'_1}{w'_1}. \end{aligned} \quad (4.38)$$

After imposing the identification $u'_{as} = u_{as}$, we find the new parameters to be given by

$$\begin{aligned} \varepsilon'_1 &= \frac{\varepsilon_1}{\sqrt{\gamma}}, & w'_1 &= -\sqrt{\gamma}w_1, & \cosh C'_1 &= -\sinh C_1, \\ \varepsilon'_2 &= \frac{\varepsilon_2}{\sqrt{\gamma}}, & w'_2 &= -\frac{w_2}{\sqrt{\gamma}}, & \cosh C'_2 &= \sinh C_2. \end{aligned} \quad (4.39)$$

Going through the different contributions of the amplitude, we find the following results:

$$A'_{\text{free}} \cong \sqrt{2} \log \varepsilon_1 + \sqrt{2} \log \varepsilon_2 - \sqrt{2} \log \gamma, \quad (4.40)$$

$$A'_{\text{per}} - A_{\text{per}} \cong -\frac{1}{2} (i\pi + \log \gamma) \log (\varepsilon_1 \varepsilon_2) - \frac{i\pi}{2} \log \left(\frac{w_1}{w_2} \right) + \text{const.} \quad (4.41)$$

For Δ' , a small subtlety appears due to the non-trivial rotation of \tilde{u} , which gives rise to contributions $\sim \log(1 - \tilde{u})$ and $\sim \log \tilde{u}$. \tilde{u} appears explicitly in the answer. However, we will not replace it with an expression in terms of the ε_s and w_s , but just use the fact that $1 - \tilde{u} \sim \mathcal{O}(\varepsilon^2)$ as can be seen from Eq. (A.11). This allows us to drop the term $\sim \log \tilde{u}$ and we obtain

$$\Delta' - \Delta \cong -i\frac{\pi}{2} \log (\varepsilon_1 \varepsilon_2) + \frac{i\pi}{2} \log \left(\frac{w_2}{w_1} \right) - \frac{i\pi}{2} \log (1 - \tilde{u}) + \text{const.} \quad (4.42)$$

Putting all results together, and using $\log \gamma = \log |\gamma| - 3i\pi$ we find for the remainder function

$$R_{7,----} + i\delta_{7,----} = \frac{\sqrt{\lambda}}{2\pi} (e_2 \log (\varepsilon_1 \varepsilon_2) + \text{const.}), \quad (4.43)$$

which is just the sum of the remainder functions for the paths $P_{7,--+}$ and $P_{7,+--}$, presented in section 4.2 and appendix E, respectively. Exponentiating, we find our final result

$$e^{R_{7,----} + i\delta_{7,----}} \Big|_{\text{MRL}} \sim \left((1 - u_{11})(1 - u_{12}) \sqrt{\tilde{u}_{21}\tilde{u}_{31}\tilde{u}_{22}\tilde{u}_{32}} \right)^{\frac{\sqrt{\lambda}}{2\pi} e_2}, \quad (4.44)$$

where

$$\delta_{7,----} = \frac{\sqrt{\lambda}}{4} \log \left(\frac{(1 - u_{11})(1 - u_{12})}{1 - \tilde{u}} \sqrt{\tilde{u}_{21}\tilde{u}_{31}\tilde{u}_{22}\tilde{u}_{32}} \right) + \frac{\sqrt{\lambda}}{4} \log \left(\frac{\tilde{u}_{21}\tilde{u}_{32}}{\tilde{u}_{31}\tilde{u}_{22}} \right). \quad (4.45)$$

This ends our study of this path and we turn to the last remaining Regge region.

4.4 Remainder function in the Regge region $(-+-)$

In section 2 we have identified four interesting Regge regions. The one we have not discussed so far is $P_{7,-+-}$, which we examine using the continuation

$$\begin{aligned} u_{11}(\varphi) &= e^{2i\varphi} u_{11}, & u_{21}(\varphi) &= e^{-i\varphi} u_{21}, & u_{31}(\varphi) &= e^{i\varphi} u_{31}, \\ u_{12}(\varphi) &= e^{2i\varphi} u_{12}, & u_{22}(\varphi) &= e^{i\varphi} u_{22}, & u_{32}(\varphi) &= e^{-i\varphi} u_{32}, & \tilde{u}(\varphi) &= e^{-2i\varphi} \tilde{u}. \end{aligned} \quad (4.46)$$

No deformation of paths is needed to satisfy the Gram relation and we can study the crossing solutions as before⁷. However, for this particular path we see no crossing solutions. The Y-system equations therefore remain unmodified at the endpoint of the continuation, and the remainder function is trivial up to a phase,

$$e^{R_{7,-+-} + i\delta_{7,-+-}} \Big|_{\text{MRL}} \sim 1, \quad (4.47)$$

⁷More precisely, there is a deformation of the path of \tilde{u} which satisfies the Gram relation and has the same winding number as the naive path. Since \tilde{u} only appears explicitly in Δ , this deformation is irrelevant.

with

$$\delta_{7,-+-} = \frac{\sqrt{\lambda}}{4} \log \left(\frac{1}{(1-\tilde{u})} \frac{1}{\tilde{u}_{22}\tilde{u}_{31}} \right), \quad (4.48)$$

which arises from the continuation of Δ . This is a rather surprising result, as we expected to see a contribution of all three cuts, as predicted by the weak coupling analysis (cf. section 2.4). It may, however, be that our choice of path is too naive for this region. For example, it is conceivable that this region should rather be probed by first following the path $P_{7,---}$ and only then flipping the middle gluon back up. Since crossing solutions occur for $P_{7,---}$ it would be interesting to see if those solutions cross back to give the trivial result Eq. (4.47) when flipping the middle gluon back up or if we find a different result. It should be noted that this issue is not present in the weak coupling description where the various regions can be studied without specifying a path which connects them.

5 Conclusions and outlook

In this paper, we have presented a general algorithm for the calculation of n -gluon scattering amplitudes in strongly coupled $\mathcal{N} = 4$ SYM in various multi-Regge regions. It is based on the central observation that the multi-Regge limit of gauge theory corresponds to the infrared or large mass limit of the TBA equations that describe the strong coupling regime. In this limit, the quantum fluctuations of the one-dimensional auxiliary integrable system can be neglected which leads to drastic simplifications. In particular, the integral equations that describe excitations of the one-dimensional system are replaced by a set of algebraic Bethe Ansatz equations and the energy of excitations is evaluated as the sum of bare energies. These general observations are highly relevant for the evaluation of Regge cut contributions at strong coupling since such cut contributions can be argued to be associated with special excitations of the auxiliary one-dimensional quantum systems. Once the relevant solution of the Bethe Ansatz equations has been identified, one can build the associated Y-functions, reconstruct the cross ratios and compute the free energy and thereby the remainder function at strong coupling.

A crucial ingredient in this program is to decide which solution of the Bethe Ansatz is actually relevant for any given multi-Regge region. At the moment we do that by analytically continuing the cross ratios along a prescribed path and following the solutions of $\tilde{Y}_{a,s}(\theta) = -1$ numerically. We characterized the paths in section 2.3. The main difficulty lies in finding paths which are compatible with the conformal Gram relations. Constructing these paths has to be done case-by-case so far and we showed an explicit example for the 7-point case. Finding paths for a general number of gluons would require a better understanding of the conformal Gram relations for arbitrary n . The numerical analysis is explained in section 3. This analysis, too, has to be carried out for each Regge region separately. We would like to stress again that the numerical analysis just provides discrete data, namely which solutions $\tilde{Y}_{a,s}(\theta) = -1$ cross the integration contour. The calculation of the remainder function is therefore not limited by numerical accuracy.

As specific examples of our algorithm, we calculate the 7-gluon amplitude in four Regge regions. For the remainder functions $R_{7,-++}$, $R_{7,+--}$ and $R_{7,---}$ we find that the result can be expressed only using the functions which appear already in the 6-gluon case for the region $R_{6,---}$.

This is in remarkable agreement with the weak-coupling predictions presented in section 2.4 and strengthens the belief that the analytic structure of the scattering amplitude as predicted by Regge theory is preserved at any value of the coupling constant.

Our findings for the remainder function $R_{7,-+-}$ disagree with the weak-coupling predictions - while we obtain a trivial remainder function (up to a phase), we expected to find contributions of three Regge cuts. As stated in section 4.4, we think that this mismatch might arise because the path we have chosen is too naive. It may well be that instead of going to the region $(-+-)$ immediately, this particular region should rather be probed by a stepwise continuation, first going to the region $(---)$ and then flipping the middle gluon back up. Since we know that crossing solutions occur for the path $P_{7,---}$ it would be interesting to see whether those solutions cross back to give a trivial remainder function when flipping the middle gluon back up or whether the remainder function at strong coupling is indeed sensitive to the way the continuation is performed. This problem will be addressed in the future.

From our results, many ideas for future research emerge. For example, it would be very interesting to study the 8-gluon amplitude. In this case it is expected from the weak-coupling perspective that in some Regge regions, the functions describing the 6-gluon case are no longer sufficient to describe the remainder function. This is due to the appearance of a new state which physically corresponds to a bound state of three Reggeons. It would therefore be relevant to understand if and how this new state shows up from the strong coupling perspective. Furthermore, since our 7-point results can be expressed through the functions appearing already in the 6-point amplitude it would be interesting to see if our results can be related to the conjectured expressions of [54].

Acknowledgments

We would like to thank Benjamin Basso, Simon Caron-Huot, Yasuyuki Hatsuda, Andrey Kormilitzin, Lev Lipatov, Arthur Lipstein and Amit Sever for valuable discussions. This work was supported by the SFB676. The research leading to these results has also received funding from the People Programme (Marie Curie Actions) of the European Union's Seventh Framework Programme FP7/2007-2013/ under REA Grant Agreement No 317089 (GATIS).

A Conformal Gram relations

For a general scattering process involving n particles, there are $3n - 10$ independent Mandelstam invariants. As we review in the main text, we can build many more Mandelstam invariants $p_i p_j$ from the n four-momenta of the external gluons. Due to this mismatch, there have to be relations among these Lorentz invariants. To find additional relations, we have to recall that in a four-dimensional space there can be at most four linearly independent vectors. Every additional vector can then be expressed as a linear combination of these four basis vectors. Without loss of generality, let us choose the momentum vectors p_1, \dots, p_4 to be a basis. We then have relations

$$\sum_i^{1..4,l} c_i p_i = 0, \quad (\text{A.1})$$

for coefficients c_i and $l = 5, \dots, n - 1$.⁸ Multiplication with $2p_j$ gives rise to relations among the Lorentz invariants. The condition that these relations have non-trivial solutions for the c_i can be cast into a different form by writing down the $(n - 1) \times (n - 1)$ -matrix of inner products of the momenta,

$$P = \begin{pmatrix} 0 & p_1 p_2 & p_1 p_3 & \cdots & p_1 p_{n-1} \\ p_2 p_1 & 0 & p_2 p_3 & \cdots & p_2 p_{n-1} \\ p_3 p_1 & p_3 p_2 & 0 & \cdots & p_3 p_{n-1} \\ \vdots & \vdots & \vdots & \ddots & \vdots \\ p_{n-1} p_1 & p_{n-1} p_2 & p_{n-1} p_3 & \cdots & 0 \end{pmatrix}, \quad (\text{A.2})$$

where the main diagonal contains only zeros, since we are scattering massless gluons. Since we chose p_1, \dots, p_4 to be a basis, these vectors are linearly independent, which is equivalent to saying that the upper left 4×4 -minor

$$\begin{vmatrix} 0 & p_1 p_2 & p_1 p_3 & p_1 p_4 \\ p_2 p_1 & 0 & p_2 p_3 & p_2 p_4 \\ p_3 p_1 & p_3 p_2 & 0 & p_3 p_4 \\ p_4 p_1 & p_4 p_2 & p_4 p_3 & 0 \end{vmatrix} \neq 0 \quad (\text{A.3})$$

does not vanish. Linear dependence of additional vectors then translates into the statement that every 5×5 -minor we can build by adding a column and a row of Eq. (A.2) to the minor Eq. (A.3) has to vanish,

$$\begin{vmatrix} 0 & p_1 p_2 & p_1 p_3 & p_1 p_4 & p_1 p_k \\ p_2 p_1 & 0 & p_2 p_3 & p_2 p_4 & p_2 p_k \\ p_3 p_1 & p_3 p_2 & 0 & p_3 p_4 & p_3 p_k \\ p_4 p_1 & p_4 p_2 & p_4 p_3 & 0 & p_4 p_k \\ p_l p_1 & p_l p_2 & p_l p_3 & p_l p_4 & p_l p_k \end{vmatrix} = 0. \quad (\text{A.4})$$

These relations are called *Gram determinant relations*. Since the coefficient matrix Eq. (A.2) is symmetric, this gives rise to $\frac{1}{2}(n - 4)(n - 5)$ relations. In total, we then have

$$\frac{n(n - 3)}{2} - \frac{(n - 5)(n - 4)}{2} = 3n - 10 \quad (\text{A.5})$$

invariants left, which is exactly the number of independent variables.

This, however, is not good enough for our given problem. In the above description we have only considered Lorentz symmetry of the variables. However, since the remainder function in $\mathcal{N} = 4$ SYM is dual conformal invariant, non-trivial kinematic information has to be expressed by conformal cross ratios. We therefore face the problem of writing down Gram relations that obey dual conformal symmetry. This problem is solved in [70].

As a first step, we change from momentum variables to the dual variables $p_i = x_{i-1} - x_i$. Of course, everything we said above still applies to these variables. We then lift four-dimensional momentum space to a six-dimensional space on which the four-dimensional dual conformal

⁸The vector p_n which is not considered here can always be expressed through the other momenta via overall momentum conservation.

symmetry $\text{SO}(4, 2)$ is realized as rotation symmetry of the null vectors $X_i^\mu := (1, x_i^2, x_i^\mu)$. Note that these vectors are denoted in light-cone coordinates, such that

$$X_i^2 = 2(1 \cdot x_i^2) - 2x_i^\mu x_{i\mu} = 0, \quad (\text{A.6})$$

as well as

$$X_i \cdot X_j = x_j^2 + x_i^2 - 2x_i \cdot x_j = (x_i - x_j)^2 = x_{i,j}^2. \quad (\text{A.7})$$

Since we are in six-dimensional space, at most six vectors X_i can be linearly independent. Without loss of generality, we choose X_1, \dots, X_6 as basis vectors. Following the same arguments as above, we find $\frac{1}{2}(n-5)(n-6)$ conditions of the form

$$\text{Gram}(1, 2, 3, 4, 5, 6, j, k) = 0, \quad (\text{A.8})$$

where the above notation indicates that the 7×7 -minor built from the six basis vectors as well as row j and column k vanishes. These relations give rise to polynomial equations in the $x_{i,j}^2$ which are dual conformally invariant by construction. Having found the relations in the $x_{i,j}^2$ we can use Eqs. (2.5)-(2.7) to rewrite the relations in terms of the cross ratios. For $n = 7$ external gluons the only relation reads

$$a\tilde{u}^2 + b\tilde{u} + c = 0 \quad (\text{A.9})$$

with lengthy coefficients

$$\begin{aligned} a &= u_{11}u_{12}(-1 + u_{12}u_{21} + u_{11}u_{32}), \\ b &= -\frac{1}{2} + u_{11} + \frac{1}{2}u_{11}u_{12} + u_{12}u_{21} - 2u_{11}u_{12}u_{21} - u_{12}^2u_{21} + u_{22} - u_{11}u_{22} \\ &\quad - 2u_{12}u_{21}u_{22} + u_{11}u_{12}u_{21}u_{22} + u_{12}^2u_{21}^2u_{22} - \frac{1}{2}u_{22}u_{31} + u_{12}u_{21}u_{22}u_{31} \\ &\quad + \frac{1}{2}u_{11}u_{12}u_{21}u_{32} + \frac{1}{2}u_{11}u_{12}u_{21}u_{22}u_{31}u_{32} + (\text{target} \leftrightarrow \text{projectile}), \\ c &= \frac{1}{2} - u_{11} - u_{21} + u_{11}u_{21} + u_{12}u_{21} - u_{22} + u_{11}u_{22} + u_{21}u_{22} - u_{11}u_{21}u_{22} \\ &\quad + u_{12}u_{21}u_{22} - u_{12}u_{21}^2u_{22} + \frac{1}{2}u_{22}u_{31} + u_{21}u_{22}u_{31} - 2u_{12}u_{21}u_{22}u_{31} \\ &\quad - u_{21}u_{22}^2u_{31} + u_{12}u_{21}^2u_{22}^2u_{31} + \frac{1}{2}u_{21}u_{32} - u_{11}u_{21}u_{32} - u_{21}u_{22}u_{31}u_{32} \\ &\quad + u_{11}u_{21}u_{22}u_{31}u_{32} + \frac{1}{2}u_{21}u_{22}^2u_{31}^2u_{32} + (\text{target} \leftrightarrow \text{projectile}), \end{aligned} \quad (\text{A.10})$$

where (target \leftrightarrow projectile) means that the same expression after applying a target-projectile transformation (cf. Eq. (2.8)), including the constant terms, should be added. This relation simplifies when approaching the multi-Regge limit. In fact, setting all small cross ratios to zero, $u_{2s} = u_{3s} = 0$, in Eq. (A.9) we find

$$0 = (\tilde{u} - 1)(1 - u_{11} - u_{12} + u_{11}u_{12}\tilde{u}). \quad (\text{A.11})$$

B The remainder function in the Euclidean regime

In this appendix we show that the remainder function of the 7-point amplitude is trivial in the Euclidean region. To do so, we use Eqs. (3.28) and (3.22) to rewrite all contributions of the remainder function in terms of the variables ε_s and w_s . Let us begin with A_{free} . Remember that in the large $|m_s|$ -regime the integrals in Eqs. (3.4)-(3.6) can be neglected, which leads to the following schematic form of the integrals appearing in A_{free} :

$$\frac{|m_s|}{2\pi} \int d\theta \cosh \theta \log \left(1 + \tilde{Y}_{a,s}(\theta) \right) \approx \frac{|m_s|}{2\pi} \int d\theta \cosh \theta e^{-|m_s| \cosh \theta} = \frac{|m_s|}{\pi} K_1(|m_s|), \quad (\text{B.1})$$

where $K_1(x)$ is a modified Bessel function of the second kind [71]. Using its large x -asymptotics,

$$xK_1(x) \sim \sqrt{\frac{\pi x}{2}} e^{-x}, \quad (\text{B.2})$$

as well as

$$|m_s| = (\log^2 \varepsilon_s + \log^2 w_s)^{\frac{1}{2}} \approx -\log \varepsilon_s, \quad (\text{B.3})$$

we see that the above integral Eq. (B.1) is of $\mathcal{O}(\varepsilon \log \varepsilon)$ and therefore vanishes in the $\varepsilon \rightarrow 0$ limit. Hence, A_{free} does not contribute in this limit. Next we study A_{per} . Starting from Eq. (3.18) and using Eq. (3.22), we find that

$$\begin{aligned} A_{\text{per}} = & \frac{1}{2} (\log^2 \varepsilon_1 + \log^2 w_1 + \log^2 \varepsilon_2 + \log^2 w_2 \\ & + \log \varepsilon_1 \log \varepsilon_2 + \log w_1 \log w_2 + \log \varepsilon_2 \log w_1 - \log \varepsilon_1 \log w_2). \end{aligned}$$

For the last remaining term of the remainder function, $A_{\text{BDS-like}} - A_{\text{BDS}}$, we use Eq. (3.28) in Eq. (3.17), expand in ε_s and keep only the leading terms, finding

$$\begin{aligned} \Delta = & -\frac{\pi^2}{6} - \frac{1}{2} (\log^2 \varepsilon_1 + \log^2 w_1 + \log^2 \varepsilon_2 + \log^2 w_2) \\ & - \frac{1}{2} (\log \varepsilon_1 \log \varepsilon_2 - \log \varepsilon_1 \log w_2 + \log \varepsilon_2 \log w_1 + \log w_1 \log w_2). \end{aligned} \quad (\text{B.4})$$

Summing all terms, we find that only a constant remainder function remains, as it must. It should be noted that this constant, $-\frac{\pi^2}{6}$, comes solely from the leading term in the expansion of the $\text{Li}_2(1 - u_i)$, which occur with opposite sign in A_{BDS} . Hence, this constant will cancel in the full amplitude.

C Kernels of the rewritten Y-system

In this appendix we spell out the Y-system kernels $\mathcal{K}_{s,s'}^{a,a'}$ of the rewritten Y-system Eqs. (4.6)-(4.8), which we use in the numerical analysis of A_{free} . $K_i(x)$ denote the kernels of the standard Y-system (cf. Eq. (3.10)). In the following, $s \pm 1$ denotes the unique possible choice for s' in a

given kernel. Furthermore, if a formula holds for both $a' = 1$ and $a' = 3$ we just write $a' = 2 \pm 1$.

$$\begin{aligned}
\mathcal{K}_{s,s}^{1,2\pm 1}(\theta, \theta') &= K_1(\theta') \cosh \theta - K_1(\theta - \theta') \\
\mathcal{K}_{s,s}^{1,2}(\theta, \theta') &= K_2(\theta') \cosh \theta - K_2(\theta - \theta') \\
\mathcal{K}_{s,s\pm 1}^{1,2}(\theta, \theta') &= -K_1(-\theta' + i\phi_s - i\phi_{s\pm 1}) \cosh \theta + K_1(\theta - \theta' + i\phi_s - i\phi_{s\pm 1}) \\
\mathcal{K}_{s,s\pm 1}^{1,1}(\theta, \theta') &= \frac{1}{2} (K_2(\theta - \theta' + i\phi_s - i\phi_{s\pm 1}) - K_2(-\theta' + i\phi_s - i\phi_{s\pm 1}) \cosh \theta) \\
&\quad + \frac{1}{2} (-1)^{s+1} (K_3(\theta - \theta' + i\phi_s - i\phi_{s\pm 1}) - K_3(-\theta' + i\phi_s - i\phi_{s\pm 1})) \\
\mathcal{K}_{s,s\pm 1}^{1,3}(\theta, \theta') &= \frac{1}{2} (K_2(\theta - \theta' + i\phi_s - i\phi_{s\pm 1}) - K_2(-\theta' + i\phi_s - i\phi_{s\pm 1}) \cosh \theta) \\
&\quad + \frac{1}{2} (-1)^s (K_3(\theta - \theta' + i\phi_s - i\phi_{s\pm 1}) - K_3(-\theta' + i\phi_s - i\phi_{s\pm 1})) \\
\mathcal{K}_{s,s}^{2,2\pm 1}(\theta, \theta') &= \sqrt{2} K_1(\theta') \cosh \theta - K_2(\theta - \theta') \\
\mathcal{K}_{s,s}^{2,2}(\theta, \theta') &= \sqrt{2} K_2(\theta') \cosh \theta - 2K_1(\theta - \theta') \\
\mathcal{K}_{s,s\pm 1}^{2,2}(\theta, \theta') &= -\sqrt{2} K_1(-\theta' + i\phi_s - i\phi_{s\pm 1}) \cosh \theta + K_2(\theta - \theta' + i\phi_s - i\phi_{s\pm 1}) \\
\mathcal{K}_{s,s\pm 1}^{2,2\pm 1}(\theta, \theta') &= -\frac{1}{\sqrt{2}} K_2(-\theta' + i\phi_s - i\phi_{s\pm 1}) \cosh \theta + K_1(\theta - \theta' + i\phi_s - i\phi_{s\pm 1}) \\
\mathcal{K}_{s,s}^{3,2\pm 1}(\theta, \theta') &= K_1(\theta') \cosh \theta - K_1(\theta - \theta') \\
\mathcal{K}_{s,s}^{3,2}(\theta, \theta') &= K_2(\theta') \cosh \theta - K_2(\theta - \theta') \\
\mathcal{K}_{s,s\pm 1}^{3,2}(\theta, \theta') &= -K_1(-\theta' + i\phi_s - i\phi_{s\pm 1}) \cosh \theta + K_1(\theta - \theta' + i\phi_s - i\phi_{s\pm 1}) \\
\mathcal{K}_{s,s\pm 1}^{3,1}(\theta, \theta') &= \frac{1}{2} (K_2(\theta - \theta' + i\phi_s - i\phi_{s\pm 1}) - K_2(-\theta' + i\phi_s - i\phi_{s\pm 1}) \cosh \theta) \\
&\quad + \frac{1}{2} (-1)^s (K_3(\theta - \theta' + i\phi_s - i\phi_{s\pm 1}) - K_3(-\theta' + i\phi_s - i\phi_{s\pm 1})) \\
\mathcal{K}_{s,s\pm 1}^{3,3}(\theta, \theta') &= \frac{1}{2} (K_2(\theta - \theta' + i\phi_s - i\phi_{s\pm 1}) - K_2(-\theta' + i\phi_s - i\phi_{s\pm 1}) \cosh \theta) \\
&\quad + \frac{1}{2} (-1)^{s+1} (K_3(\theta - \theta' + i\phi_s - i\phi_{s\pm 1}) - K_3(-\theta' + i\phi_s - i\phi_{s\pm 1}))
\end{aligned}$$

D S-matrices

For the new set of kernels written out in appendix C, we have to determine the corresponding S-matrices. However, this is simple because the new kernels are linear combinations of the original kernels, possibly with prefactors. Therefore, the new S-matrices too should be given in terms of the original S-matrices Eqs. (3.32). Recall the original definition of the S-matrices,

$$-2\pi i K(\theta) =: \partial_\theta \log S(\theta). \quad (\text{D.1})$$

Since the new kernels are now in general functions of both θ, θ' and not just their difference, we have to extend this definition in the following way:

$$-2\pi i K(\theta, \theta') =: \partial_{\theta'} \log S(\theta, \theta') \quad (\text{D.2})$$

This allows us to pick up the residue contributions in a very simple way, as before. Using this definition, we see that for a kernel of the schematic form

$$K(\theta, \theta') = f(\theta)K_1(\theta, \theta') + g(\theta)K_2(\theta, \theta') + \dots \quad (\text{D.3})$$

the S-matrix is given by

$$S(\theta, \theta') = S_1(\theta, \theta')^{f(\theta)} \cdot S_2(\theta, \theta')^{g(\theta)} \cdot \dots \quad (\text{D.4})$$

As a specific example, we spell out the S-matrices for a crossed solution of $\tilde{Y}_{3,1}$ in the rewritten Y-system below:

$$\begin{aligned} S_{1,1}^{2,3}(\theta, \theta') &= S_1(\theta')^{\sqrt{2} \cosh \theta} S_2(\theta - \theta') \\ S_{1,1}^{2\pm 1,3}(\theta, \theta') &= S_1(\theta')^{\cosh \theta} S_1(\theta - \theta') \\ S_{2,1}^{1,3}(\theta, \theta') &= \frac{S_2(-\theta' + i\phi_2 - i\phi_1)^{\frac{1}{2} \cosh \theta} S_3(-\theta' + i\phi_2 - i\phi_1)^{\frac{1}{2}}}{S_2(\theta - \theta' + i\phi_2 - i\phi_1)^{\frac{1}{2}} S_3(\theta - \theta' + i\phi_2 - i\phi_1)^{\frac{1}{2}}} \\ S_{2,1}^{2,3}(\theta, \theta') &= S_2(\theta' - i\phi_2 + i\phi_1)^{-\frac{1}{\sqrt{2}} \cosh \theta} S_1(\theta - \theta' + i\phi_2 - i\phi_1)^{-1} \\ S_{2,1}^{3,3}(\theta, \theta') &= \frac{S_2(-\theta' + i\phi_2 - i\phi_1)^{\frac{1}{2} \cosh \theta} S_3(\theta - \theta' + i\phi_2 - i\phi_1)^{\frac{1}{2}}}{S_2(\theta - \theta' + i\phi_2 - i\phi_1)^{\frac{1}{2}} S_3(-\theta' + i\phi_2 - i\phi_1)^{\frac{1}{2}}} \end{aligned} \quad (\text{D.5})$$

Similarly, we obtain all the other S-matrices from the kernels of appendix C. We refrain from spelling them out here explicitly.

E Remainder function in the Regge region (+ - -)

In this section we will briefly show the calculation for the path $P_{7,+--}$ of the cross ratios that was defined in Eq. (2.22). The calculation proceeds along the same steps as the one in section 4. Therefore, we only highlight the differences in the following. For the numerical analysis, we again have to determine the paths of the variables Eq. (4.2) under the continuation Eq. (2.22). We find the results depicted in figure 8. Having found the paths of the driving terms, we can follow the solutions $\tilde{Y}_{a,s} = -1$ during the continuation, leading to the results shown in figure 9. We see that for the path $P_{7,+--}$, two solutions of $\tilde{Y}_{3,1}$ cross the real axis and approach $\pm i\frac{\pi}{4}$, which can again be confirmed by an analytic argument using the endpoint conditions Eq. (3.37). Furthermore, we find a pair of solutions of $\tilde{Y}_{2,1}$ which approaches the real axis but never crosses. As before, these solutions do not contribute to the remainder function. Thus, after neglecting the integrals, the Y-system after the continuation is given by

$$Y'_{1,s} = \left(e^{-|m_s|' \cosh(\theta - i\phi'_s) - C'_s} \right) \frac{S_{s,1}^{1,3}(\theta + i\frac{\pi}{4} - i\phi'_1)}{S_{s,1}^{1,3}(\theta - i\frac{\pi}{4} - i\phi'_1)}, \quad (\text{E.1})$$

$$Y'_{2,s} = \left(e^{-\sqrt{2}|m_s|' \cosh(\theta - i\phi'_s)} \right) \frac{S_{s,1}^{2,3}(\theta + i\frac{\pi}{4} - i\phi'_1)}{S_{s,1}^{2,3}(\theta - i\frac{\pi}{4} - i\phi'_1)}, \quad (\text{E.2})$$

$$Y'_{3,s} = \left(e^{-|m_s|' \cosh(\theta - i\phi'_s) + C'_s} \right) \frac{S_{s,1}^{3,3}(\theta + i\frac{\pi}{4} - i\phi'_1)}{S_{s,1}^{3,3}(\theta - i\frac{\pi}{4} - i\phi'_1)}, \quad (\text{E.3})$$

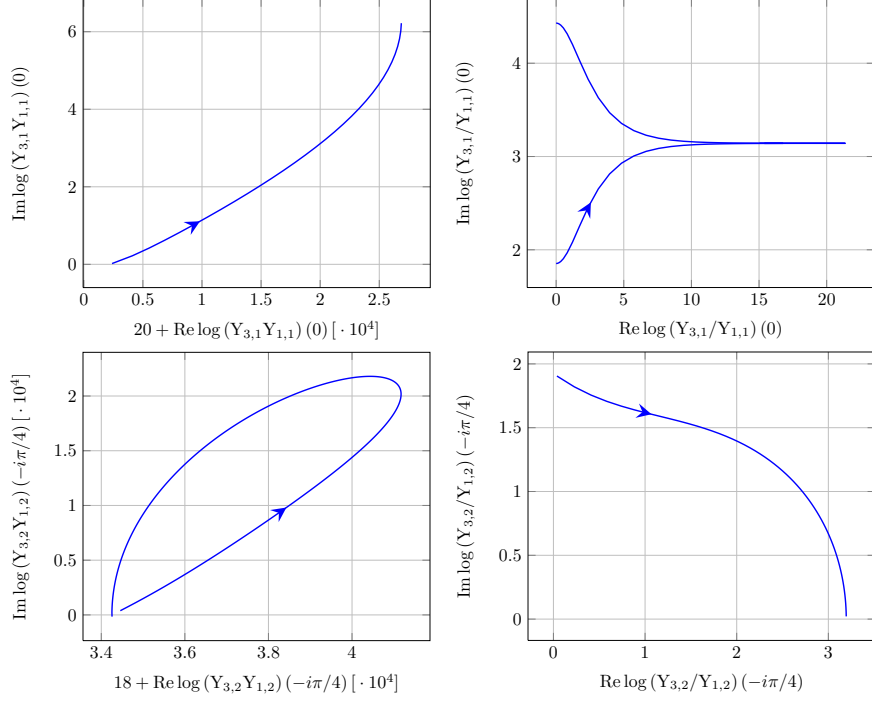


Figure 8. Continuation of the driving terms for the path Eq. (2.22). Note that some axes have been rescaled and shifted. The direction of growing φ is indicated by the arrows. The plots shown correspond to the parameter choice $|m_1| = 10$, $|m_2| = 9$, $C_1 = \operatorname{arccosh}(\frac{3}{5})$, $C_2 = \operatorname{arccosh}(\frac{4}{7})$ at the starting point.

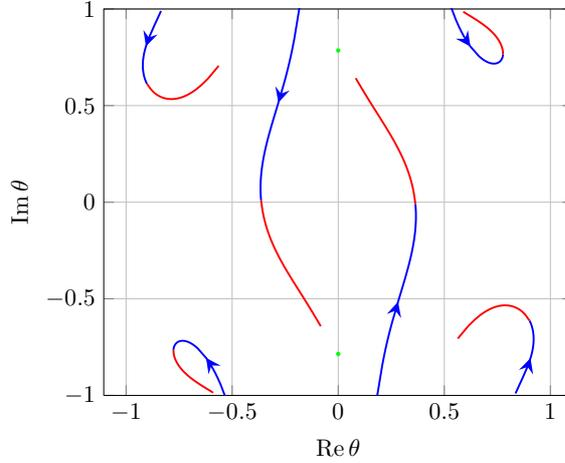


Figure 9. Paths followed by the solutions of $\tilde{Y}_{3,1}(\theta) = -1$ during the continuation Eq. (2.22). We find that one pair of solutions crosses the real axis. The direction of movement is indicated by arrows on the plot. We change the color of the curve when the pair of solutions crosses the integration contour.

with the S-matrices spelled out in appendix D. With this Y-system we determine the cross ratios after continuation to be

$$\begin{aligned}
 u'_{11} &= 1 + \varepsilon'_2 \left(w'_2 + \frac{1}{\gamma w'_2} + 2 \frac{1}{\sqrt{-\gamma}} \sinh C'_2 \right), & u'_{21} &= -w'_2 \varepsilon'_2, & u'_{31} &= -\frac{1}{\gamma} \frac{\varepsilon'_2}{w'_2}, \\
 u'_{12} &= 1 - \gamma \varepsilon'_1 \left(w'_1 + \frac{1}{w'_1} - 2 \cosh C'_1 \right), & u'_{22} &= \gamma w'_1 \varepsilon'_1, & u'_{32} &= \gamma \frac{\varepsilon'_1}{w'_1}.
 \end{aligned}$$

Setting $u'_{21} = -u_{21}$, $u'_{31} = -u_{31}$ and $u'_{as} = u_{as}$ for the remaining cross ratios we find

$$\begin{aligned} \varepsilon'_1 &= \frac{1}{\gamma}\varepsilon_1, & w'_1 &= w_1, & \cosh C'_1 &= -\cosh C_1, \\ \varepsilon'_2 &= \sqrt{\gamma}\varepsilon_2, & w'_2 &= \frac{1}{\sqrt{\gamma}}w_2, & \cosh C'_2 &= \sqrt{1 - \left(w_2 + \frac{1}{w_2} + \cosh C_2\right)^2} \end{aligned} \quad (\text{E.4})$$

for the analytically continued auxiliary parameters. The rest of the calculation goes through as for the path $P_{7,-,+}$ and we find the result

$$e^{\text{R}_{7,+++} + i\delta_{7,+-}} \Big|_{\text{MRL}} \sim \left(-(1 - u_{12})\sqrt{\tilde{u}_{22}\tilde{u}_{32}} \right)^{\frac{\sqrt{\lambda}}{2\pi}e_2} \quad (\text{E.5})$$

where

$$\delta_{7,+-} = \frac{\sqrt{\lambda}}{4} \log \left(\sqrt{\tilde{u}_{22}\tilde{u}_{32}} \right). \quad (\text{E.6})$$

This result is consistent with the target-projectile symmetry which relates paths $P_{7,-,+}$ and $P_{7,+-}$.

References

- [1] J. Bartels, V. Schomerus and M. Sprenger, JHEP **1410** (2014) 67 [arXiv:1405.3658 [hep-th]].
- [2] Z. Bern, L. J. Dixon and V. A. Smirnov, Phys. Rev. D **72** (2005) 085001 [hep-th/0505205].
- [3] L. F. Alday and J. Maldacena, JHEP **0711** (2007) 068 [arXiv:0710.1060 [hep-th]].
- [4] J. Bartels, L. N. Lipatov and A. Sabio Vera, Phys. Rev. D **80** (2009) 045002 [arXiv:0802.2065 [hep-th]].
- [5] J. Bartels, L. N. Lipatov and A. Sabio Vera, Eur. Phys. J. C **65** (2010) 587 [arXiv:0807.0894 [hep-th]].
- [6] A. B. Goncharov, M. Spradlin, C. Vergu and A. Volovich, Phys. Rev. Lett. **105** (2010) 151605 [arXiv:1006.5703 [hep-th]].
- [7] L. J. Dixon, J. M. Drummond, M. von Hippel and J. Pennington, JHEP **1312** (2013) 049 [arXiv:1308.2276 [hep-th]].
- [8] L. J. Dixon, J. M. Drummond, C. Duhr and J. Pennington, JHEP **1406** (2014) 116 [arXiv:1402.3300 [hep-th]].
- [9] S. Caron-Huot, JHEP **1112** (2011) 066 [arXiv:1105.5606 [hep-th]].
- [10] J. Golden and M. Spradlin, JHEP **1408** (2014) 154 [arXiv:1406.2055 [hep-th]].
- [11] B. Basso, A. Sever and P. Vieira, Phys. Rev. Lett. **111** (2013) 9, 091602 [arXiv:1303.1396 [hep-th]].
- [12] B. Basso, A. Sever and P. Vieira, JHEP **1401** (2014) 008 [arXiv:1306.2058 [hep-th]].
- [13] B. Basso, A. Sever and P. Vieira, JHEP **1408** (2014) 085 [arXiv:1402.3307 [hep-th]].
- [14] B. Basso, A. Sever and P. Vieira, JHEP **1409** (2014) 149 [arXiv:1407.1736 [hep-th]].
- [15] N. Beisert, C. Ahn, L. F. Alday, Z. Bajnok, J. M. Drummond, L. Freyhult, N. Gromov and R. A. Janik *et al.*, Lett. Math. Phys. **99** (2012) 3 [arXiv:1012.3982 [hep-th]].

- [16] N. Gromov, V. Kazakov, S. Leurent and D. Volin, *Phys. Rev. Lett.* **112** (2014) 1, 011602 [arXiv:1305.1939 [hep-th]].
- [17] N. Gromov, V. Kazakov, S. Leurent and D. Volin, arXiv:1405.4857 [hep-th].
- [18] J. A. Minahan and K. Zarembo, *JHEP* **0303** (2003) 013 [hep-th/0212208].
- [19] N. Beisert, C. Kristjansen and M. Staudacher, *Nucl. Phys. B* **664** (2003) 131 [hep-th/0303060].
- [20] N. Beisert, *Nucl. Phys. B* **676** (2004) 3 [hep-th/0307015].
- [21] V. A. Kazakov, A. Marshakov, J. A. Minahan and K. Zarembo, *JHEP* **0405** (2004) 024 [hep-th/0402207].
- [22] J. M. Maldacena, *Int. J. Theor. Phys.* **38** (1999) 1113 [*Adv. Theor. Math. Phys.* **2** (1998) 231] [hep-th/9711200].
- [23] E. Witten, *Adv. Theor. Math. Phys.* **2** (1998) 253 [hep-th/9802150].
- [24] S. S. Gubser, I. R. Klebanov and A. M. Polyakov, *Phys. Lett. B* **428**, 105 (1998) [hep-th/9802109].
- [25] G. Arutyunov, S. Frolov and M. Staudacher, *JHEP* **0410** (2004) 016 [hep-th/0406256].
- [26] N. Beisert and A. A. Tseytlin, *Phys. Lett. B* **629** (2005) 102 [hep-th/0509084].
- [27] R. Hernandez and E. Lopez, *JHEP* **0607** (2006) 004 [hep-th/0603204].
- [28] L. Freyhult and C. Kristjansen, *Phys. Lett. B* **638** (2006) 258 [hep-th/0604069].
- [29] N. Beisert, R. Hernandez and E. Lopez, *JHEP* **0611** (2006) 070 [hep-th/0609044].
- [30] N. Beisert, B. Eden and M. Staudacher, *J. Stat. Mech.* **0701** (2007) P01021 [hep-th/0610251].
- [31] L. F. Alday and J. M. Maldacena, *JHEP* **0706** (2007) 064 [arXiv:0705.0303 [hep-th]].
- [32] L. F. Alday and J. Maldacena, *JHEP* **0911** (2009) 082 [arXiv:0904.0663 [hep-th]].
- [33] L. F. Alday, D. Gaiotto and J. Maldacena, *JHEP* **1109** (2011) 032 [arXiv:0911.4708 [hep-th]].
- [34] L. F. Alday, J. Maldacena, A. Sever and P. Vieira, *J. Phys. A* **43** (2010) 485401 [arXiv:1002.2459 [hep-th]].
- [35] P. Heslop and V. V. Khoze, *JHEP* **1011** (2010) 035 [arXiv:1007.1805 [hep-th]].
- [36] T. Goddard, P. Heslop and V. V. Khoze, *JHEP* **1210** (2012) 041 [arXiv:1205.3448 [hep-th]].
- [37] M. A. C. Torres, *Eur. Phys. J. C* **74** (2014) 2757 [arXiv:1310.6906 [hep-th]].
- [38] J. C. Toledo, arXiv:1410.5896 [hep-th].
- [39] Y. Hatsuda, K. Ito, K. Sakai and Y. Satoh, *JHEP* **1009** (2010) 064 [arXiv:1005.4487 [hep-th]].
- [40] Y. Hatsuda, K. Ito, K. Sakai and Y. Satoh, *JHEP* **1104** (2011) 100 [arXiv:1102.2477 [hep-th]].
- [41] Y. Hatsuda, K. Ito and Y. Satoh, *JHEP* **1202** (2012) 003 [arXiv:1109.5564 [hep-th]].
- [42] Y. Hatsuda, K. Ito and Y. Satoh, *JHEP* **1302** (2013) 067 [arXiv:1211.6225 [hep-th]].
- [43] L. F. Alday, D. Gaiotto, J. Maldacena, A. Sever and P. Vieira, *JHEP* **1104** (2011) 088 [arXiv:1006.2788 [hep-th]].
- [44] D. Gaiotto, J. Maldacena, A. Sever and P. Vieira, *JHEP* **1103** (2011) 092 [arXiv:1010.5009 [hep-th]].
- [45] D. Gaiotto, J. Maldacena, A. Sever and P. Vieira, *JHEP* **1112** (2011) 011 [arXiv:1102.0062 [hep-th]].

- [46] A. Sever, P. Vieira and T. Wang, JHEP **1111** (2011) 051 [arXiv:1108.1575 [hep-th]].
- [47] A. Sever, P. Vieira and T. Wang, JHEP **1212** (2012) 065 [arXiv:1208.0841 [hep-th]].
- [48] B. Basso, A. Sever and P. Vieira, arXiv:1405.6350 [hep-th].
- [49] L. D. Faddeev and G. P. Korchemsky, Phys. Lett. B **342** (1995) 311 [hep-th/9404173].
- [50] L. N. Lipatov, hep-th/9311037.
- [51] V. S. Fadin and L. N. Lipatov, Phys. Lett. B **706** (2012) 470 [arXiv:1111.0782 [hep-th]].
- [52] L. N. Lipatov and A. Prygarin, Phys. Rev. D **83** (2011) 125001 [arXiv:1011.2673 [hep-th]].
- [53] L. J. Dixon, C. Duhr and J. Pennington, JHEP **1210** (2012) 074 [arXiv:1207.0186 [hep-th]].
- [54] B. Basso, S. Caron-Huot and A. Sever, arXiv:1407.3766 [hep-th].
- [55] J. Bartels, J. Kotanski and V. Schomerus, JHEP **1101** (2011) 096 [arXiv:1009.3938 [hep-th]].
- [56] J. Bartels, V. Schomerus and M. Sprenger, JHEP **1211** (2012) 145 [arXiv:1207.4204 [hep-th]].
- [57] J. Bartels, A. Kormilitzin and L. Lipatov, Phys. Rev. D **89** (2014) 065002 [arXiv:1311.2061 [hep-th]].
- [58] L. N. Lipatov, Theor. Math. Phys. **170** (2012) 166 [arXiv:1008.1015 [hep-th]].
- [59] J. Bartels, A. Kormilitzin and L. Lipatov, in preparation
- [60] J. Bartels, A. Kormilitzin and L. Lipatov, in preparation
- [61] J. Bartels, A. Kormilitzin, L. N. Lipatov and A. Prygarin, Phys. Rev. D **86** (2012) 065026 [arXiv:1112.6366 [hep-th]].
- [62] L. N. Lipatov, J. Phys. A **42** (2009) 304020 [arXiv:0902.1444 [hep-th]].
- [63] S. E. Derkachov and A. N. Manashov, J. Phys. A **47** (2014) 305204 [arXiv:1401.7477 [math-ph]].
- [64] G. Yang, JHEP **1012** (2010) 082 [arXiv:1004.3983 [hep-th]].
- [65] J. M. Drummond, J. Henn, G. P. Korchemsky and E. Sokatchev, Nucl. Phys. B **826** (2010) 337 [arXiv:0712.1223 [hep-th]].
- [66] G. Yang, JHEP **1103** (2011) 087 [arXiv:1006.3306 [hep-th]].
- [67] P. Dorey and R. Tateo, Nucl. Phys. B **482** (1996) 639 [hep-th/9607167].
- [68] P. Dorey and R. Tateo, Nucl. Phys. B **515** (1998) 575 [hep-th/9706140].
- [69] J. Bartels, J. Kotanski, V. Schomerus and M. Sprenger, arXiv:1311.1512 [hep-th].
- [70] B. Eden, P. Heslop, G. P. Korchemsky and E. Sokatchev, Nucl. Phys. B **862** (2012) 450 [arXiv:1201.5329 [hep-th]].
- [71] M. Abramowitz and I. A. Stegun, Eds. ‘*Handbook of Mathematical Functions with Formulas, Graphs and Mathematical Tables*’ Dover Publications (1972).